October 1993 UILU-ENG-93-2243

ABSORBING BOUNDARY CONDITIONS FOR THE FINITE-DIFFERENCE TIME-DOMAIN ANALYSIS OF GUIDED-WAVE STRUCTURES

V.T. Betz
R. Mittra

Coordinated Science Laboratory
College of Engineering
UNIVERSITY OF ILLINOIS AT URBANA-CHAMPAIGN

SECURITY CLASSIFICATION OF THIS PAGE

REPORT DOCUMENTATION PAGE

Form Approved
OMB No. 0704-0188

1a. REPORT SECURITY CLASSIFICATION Unclassified	1b. RESTRICTIVE MARKINGS
2a. SECURITY CLASSIFICATION AUTHORITY	3. DISTRIBUTION / AVAILABILITY OF REPORT Approved for public release; distribution unlimited
2b. DECLASSIFICATION / DOWNGRADING SCHEDULE	
4. PERFORMING ORGANIZATION REPORT NUMBER(S) UILU-ENG-93-2243	5. MONITORING ORGANIZATION REPORT NUMBER(S)
6a. NAME OF PERFORMING ORGANIZATION Coordinated Science Lab. University of Illinois 6b. OFFICE SYMBOL (If applicable) N/A	7a. NAME OF MONITORING ORGANIZATION Office of Naval Research
6c. ADDRESS (City, State, and ZIP Code) Urbana, IL 61801	7b. ADDRESS (City, State, and ZIP Code) Arlington, VA 22217
8a. NAME OF FUNDING / SPONSORING ORGANIZATION Joint Services Electronics Program 8b. OFFICE SYMBOL (If applicable)	9. PROCUREMENT INSTRUMENT IDENTIFICATION NUMBER N00014-90-J-1270
8c. ADDRESS (City, State, and ZIP Code) Arlington, VA 22217	10. SOURCE OF FUNDING NUMBERS PROGRAM ELEMENT NO. / PROJECT NO. / TASK NO. / WORK UNIT ACCESSION NO.

11. TITLE (Include Security Classification)
Absorbing Boudnary Conditions for the Finite-Difference Time-Domain Analysis of Guided-Wave Structures.

12. PERSONAL AUTHOR(S)
V. T. Betz and R. Mittra

13a. TYPE OF REPORT	13b. TIME COVERED	14. DATE OF REPORT (Year, Month, Day)	15. PAGE COUNT
Technical	FROM _____ TO _____	1993, October, 26	58

16. SUPPLEMENTARY NOTATION

17. COSATI CODES			18. SUBJECT TERMS (Continue on reverse if necessary and identify by block number)
FIELD	GROUP	SUB-GROUP	Electromagnetics; Guided Wave Systems; Finite Difference Time Domain (FDTD); Absorbing Boundary Conditions (ABCs)

19. ABSTRACT (Continue on reverse if necessary and identify by block number)

In this work, we address the problem of truncating the computational domain of open guided wave structures analyzed by using the Finite Difference Time Domain (FDTD) Algorithm. Several different absorbing boundary conditions (ABCs) are examined and a comparative study of their performances is carried out. Both the dispersive and evanescent type of boundary conditions are discussed and the accuracies of different orders of these conditions are evaluated.

20. DISTRIBUTION / AVAILABILITY OF ABSTRACT ☒ UNCLASSIFIED/UNLIMITED ☐ SAME AS RPT. ☐ DTIC USERS	21. ABSTRACT SECURITY CLASSIFICATION Unclassified
22a. NAME OF RESPONSIBLE INDIVIDUAL	22b. TELEPHONE (Include Area Code) / 22c. OFFICE SYMBOL

DD Form 1473, JUN 86 *Previous editions are obsolete.* SECURITY CLASSIFICATION OF THIS PAGE

Absorbing Boundary Conditions for the Finite-Difference Time-Domain Analysis of Guided-Wave Structures

by

V. T. Betz and R. Mittra
Electromagnetic Communication Laboratory
University of Illinois
Urbana, IL 61801

TABLE OF CONTENTS

CHAPTER 1
INTRODUCTION

The design of the electronic packages which interface integrated circuits to circuit boards and of the circuit boards which interconnect various electronic components is becoming increasingly difficult as clock speeds rise and the density of interconnections increases. At these high clock speeds, the dispersive nature of the microstrip lines forming the circuit board, reflections from discontinuities such as bends, and cross-talk caused by the electromagnetic coupling between lines can all severely degrade signal integrity. In addition, the very large number of circuit traces in a modern circuit board, or of pins in an electronic package, means that prototyping and testing these devices is costly, and trial-and-error approaches to design are unlikely to produce acceptable results. Consequently, there is a great deal of interest in accurately characterizing circuit board and electronic packaging components via numerical electromagnetic solvers so that computer-aided design techniques can be used to efficiently optimize a product.

The Finite-Difference Time-Domain (FDTD) method [1] is an attractive technique for analyzing the performance of electronic packages and circuit boards. Since the FDTD method is a partial differential equation algorithm, no Green's function is required and, consequently, any arbitrary geometry can be simulated. Integral equation methods, in contrast, can solve only a limited class of geometrical structures for which a Green's function can be obtained and evaluated. Many other methods of analyzing microwave circuits are static or quasi-static approximations and do not fully predict the frequency response of the circuits. Frequency-domain algorithms solve the problem for only a single frequency; consequently a large number of runs must be made to determine the complete frequency response. Using the FDTD method, however, one can determine the complete frequency response of a structure by performing a Fourier transform on the time-domain waveform. Finally, the time-domain data are of considerable utility; they can provide the designer with a

clear view of how a signal propagates along a structure and of the signal integrity at each point.

Since both integrated circuit packages and circuit boards are typically open region problems, absorbing boundary conditions (ABCs) must be employed to terminate the computational space. Even small reflections from these boundaries can introduce significant errors in the computation; consequently, highly absorbing boundary conditions are essential to obtain accurate results. Several different absorbing boundary conditions have been described in the electromagnetics literature; however, most of these ABCs were designed for use with scattering and free-space radiation problems. In scattering problems, the speed of the wave incident on the ABC is known, while its direction of propagation is unknown. Furthermore, the ABCs in a scattering problem are placed sufficiently far from the scatterer that evanescent waves are negligible near them. Both integrated circuit packages and circuit boards consist primarily of guided-wave structures, and the waves impinging upon the boundaries of a simulation of a guided-wave structure are quite different. Consequently, one must use different ABCs to achieve optimal performance.

Microstrip line is by far the most common type of waveguiding structure in integrated circuit packages and circuit boards. Consequently, this thesis focuses on developing ABCs suitable for the simulation of microstrip; however, since the wave behavior generated by most waveguiding structures is similar to that of microstrip, these ABCs should perform well on most types of waveguides. Two different types of absorbing boundaries are needed to model microstrip circuits. Since microstrip line is a dispersive structure and one typically uses a broadband excitation in FDTD simulations, the walls terminating the computational domain in the longitudinal, or guiding, direction must be capable of absorbing normally incident waves with a reasonably wide range of propagation velocities. The boundary condition enforced on the side walls, which truncate the computational domain in the transverse direction, is quite different. Although the fields impinging upon the side walls are primarily evanescent, they have, nonetheless, some contribution from surface waves that

propagate outwards. Furthermore, many problems of interest involve some type of discontinuity in the microstrip, and the fields scattered by the discontinuity will, in general, contain radiated waves that propagate toward the side walls. It is essential, therefore, that the boundary condition enforced on the side walls absorbs both traveling and evanescent waves.

This thesis focuses upon finding better absorbing boundary conditions for the FDTD simulation of guided-wave structures. Chapter 2 discusses how absorbing boundary conditions can be derived by considering the Fourier space representation of solutions of the wave equation. The derivation of the ABCs tailored to guided-wave problems relies heavily on the theory presented in this chapter. The applicability to guided-wave problems of three different types of absorbing boundaries which were originally developed for scattering-type problems is also discussed.

Chapter 3 addresses the question of which ABCs are best-suited to absorbing guided waves incident on the end walls of a microstrip line. Several different ABCs are presented and described and their relative performance is compared via numerical simulations of microstrip line. Since all of these ABCs contain some input parameters, the sensitivity of the boundary conditions to the choice of parameters is investigated and optimal choices of these parameters are given. Finally, the frequency-dependent effective permittivity of a microstrip is calculated using different ABCs to terminate the end walls to demonstrate the deleterious effect that even small reflections in the time-domain data can have on frequency-domain parameters.

Chapter 4 deals with the ABCs used to terminate the side walls of a microstrip simulation. Two new boundary conditions are introduced: one which absorbs evanescent waves only, and one which absorbs both evanescent and propagating waves. Both boundary conditions are evaluated via the FDTD simulation of a uniform microstrip line. Since the combined evanescent-traveling wave ABC performs better than the evanescent ABC, a further test of this ABC is conducted by applying it to the simulation of a microstrip gap

discontinuity. The sensitivity of this ABC's performance to the chosen input parameters is explored and a computationally efficient method for determining these parameters is given.

Finally, Chapter 5 summarizes the important conclusions drawn from this research.

CHAPTER 2

DERIVATION OF ABSORBING BOUNDARY CONDITIONS FROM THE WAVE EQUATION

We wish to solve the wave equation, subject to the condition that all radiation is outgoing on at least some of the boundaries. Let us consider a problem in which the boundaries are the faces of a cube, as this is the typical case when one uses the FDTD method to solve a problem. Further, let the only absorbing boundary be at the x = 0 plane; once we derive an absorbing boundary for this wall, the generalization to the five other boundaries is straightforward. The treatment followed here is similar to that of Engquist and Majda [2], but has been generalized to three dimensions and the notation here will be more familiar to electrical engineers.

2.1 A Perfect Absorbing Boundary Condition Found via Plane-Wave Expansion

We must solve the wave equation

$$\nabla^2 E - \frac{1}{c^2}\frac{\partial^2 E}{\partial t^2} = \frac{\partial^2 E}{\partial x^2} + \frac{\partial^2 E}{\partial y^2} + \frac{\partial^2 E}{\partial z^2} - \frac{1}{c^2}\frac{\partial^2 E}{\partial t^2} = 0 \tag{2.1}$$

in the x > 0 half-space, subject to the condition that there are only outgoing waves (waves traveling to the left) at the x = 0 plane. An important special group of solutions consists of the plane waves

$$E(x,y,z,t) = e^{j(\omega t + k_x x + k_y y + k_z z)} \tag{2.2}$$

where ω is greater than zero; k_x must be greater than zero to satisfy the outgoing wave boundary condition at x = 0; and k_y and k_z can be either positive or negative. From the dispersion relation

$$k_x^2 + k_y^2 + k_z^2 = \frac{\omega^2}{c^2} = k^2 \tag{2.3}$$

one can rewrite the plane waves which satisfy the outgoing wave condition at x = 0 as

$$E(x,y,z) = e^{j\left(\omega t + \sqrt{\frac{\omega^2}{c^2} - k_y^2 - k_z^2}\, x + k_y y + k_z z\right)}. \tag{2.4}$$

Clearly this plane wave will satisfy the boundary condition

$$\left(\frac{\partial}{\partial x} - j\sqrt{\frac{\omega^2}{c^2} - k_y^2 - k_z^2}\right) E(x,y,z)\Big|_{x=0} = 0 \tag{2.5}$$

while incoming plane waves, which are of the form

$$E(x,y,z) = e^{j\left(\omega t - \sqrt{\frac{\omega^2}{c^2} - k_y^2 - k_z^2}\, x + k_y y + k_z z\right)}, \tag{2.6}$$

will not. We thus have a boundary condition which will admit only an outgoing plane wave. Note also that (2.5) produces no reflection when the plane wave of (2.4) is incident upon it; the plane wave is *perfectly* absorbed.

Boundary condition (2.5) could be used to absorb a plane wave traveling to the left if we knew ω, k_y and k_z of the wave a priori. Unfortunately, this will not occur in FDTD analysis; if we know that the solution of a problem is a plane wave with a specific frequency, speed and direction of propagation, we need not run any numerical simulation. However, an arbitrary waveform can be formed from a superposition of an infinite number of plane waves, that is, from a Fourier integral:

$$E(x,y,z,t) = \iiint e^{j\left(\sqrt{\frac{\omega^2}{c^2} - k_y^2 - k_z^2}\, x + \omega t + k_y y + k_z z\right)} \tilde{E}(x,k_y,k_z,\omega)\, dk_y dk_z d\omega. \tag{2.7}$$

In (2.7) the ~ over $E(x,k_y,k_z,\omega)$ indicates that E(x,y,z,t) has been Fourier transformed in the y, z and t variables. Since (2.7) is a superposition of plane waves, we can apply boundary condition (2.5) to generate an ABC which will *perfectly* absorb a general wave traveling to the left:

$$\left.\frac{\partial E(x,y,z,t)}{\partial x}\right|_{x=0} - \iiint e^{j(\omega t + k_y y + k_z z)} j\sqrt{\frac{\omega^2}{c^2} - k_y^2 - k_z^2}\, \tilde{E}(0,k_y,k_z,\omega)\, dk_y dk_z d\omega = 0. \tag{2.8}$$

Unfortunately, while (2.8) is a perfect ABC in that it will completely absorb all incident radiation, it is also computationally impractical. This boundary condition is global in both

space and time; one requires field values from all previous times over the entire boundary to compute one time step at a single boundary point. In Section 2.3, therefore, our focus will be on using highly absorbing local approximations to (2.8) to develop an ABC which is computationally practical.

2.2 Pseudo-Differential Operators

A convenient and widely used shorthand uses pseudo-differential operators to express absorbing boundary conditions. Pseudo-differential operators are defined via the Fourier transform according to the rule

$$L\left(\frac{\partial}{\partial y},\frac{\partial}{\partial z},\frac{\partial}{\partial t}\right)E=\iiint e^{j\left(\omega t+k_y y+k_z z\right)}L\left(jk_y,jk_z,j\omega\right)\tilde{E}(k_y,k_z,\omega)\,dk_y dk_z d\omega \qquad (2.9)$$

where L is some operation and E is a function of y, z, and t. In other words, an equation which uses pseudo-differential operators is really defined by transforming the functions to Fourier space and replacing the derivatives with j times the appropriate wavenumber. This is a key point -- pseudo-differential operators cannot be evaluated by merely bringing the function, E, into the operator so that the derivatives act directly upon it. Pseudo-differential operators correspond to real derivatives only when you have a function multiplied by differentials because multiplication by j times the wavenumber in the Fourier domain corresponds to differentiation in the spatial domain. Other factors which arise in pseudo-differential equations, such as the square root of sums of differentials, cannot be evaluated via derivatives and have meaning only as pseudo-differential, or Fourier space, operators.

In terms of pseudo-differential operators, the boundary condition of (2.8) is

$$\left(\frac{\partial}{\partial x}-\sqrt{\frac{1}{c^2}\frac{\partial^2}{\partial t^2}-\frac{\partial^2}{\partial y^2}-\frac{\partial^2}{\partial z^2}}\right)E\Big|_{x=0}=0. \qquad (2.10)$$

The pseudo-differential equation above is not a rational formula, so it does not correspond to a partial differential equation [3]. As stated in Section 2.1, this is a global operator; we must approximate (2.10) in order to convert it to a partial differential equation which can be

implemented as a local boundary condition. Equation (2.10) is often called the one-way wave equation, since it permits propagation only in the negative x-direction. An alternative way to find (2.10) is to factor the wave equation

$$\left(\frac{\partial}{\partial x}-\sqrt{\frac{1}{c^2}\frac{\partial^2}{\partial t^2}-\frac{\partial^2}{\partial y^2}-\frac{\partial^2}{\partial z^2}}\right)\left(\frac{\partial}{\partial x}+\sqrt{\frac{1}{c^2}\frac{\partial^2}{\partial t^2}-\frac{\partial^2}{\partial y^2}-\frac{\partial^2}{\partial z^2}}\right)E=0 \tag{2.11}$$

and to realize that the two factors correspond to wave propagation in the negative and positive x-directions, respectively. Although this derivation is considerably shorter than that of Section 2.1, it does not give much insight into what these pseudo-differential operators mean or the problems which bar their direct implementation.

2.3 Approximation of the Exact Absorbing Boundary Condition: The Mur ABCs

As was stated earlier, the exact ABC of Equation (2.8) or (2.10) cannot be implemented in a computationally practical manner. Consequently, we must approximate the square-root term in (2.10). In electromagnetic FDTD analysis the most commonly used ABCs are the first- and second-order Mur [4] boundary conditions, which are equivalent to those of Engquist and Majda. By approximating the square root by the first term in its Taylor series we obtain

$$\left(\frac{\partial}{\partial x}-\frac{1}{c}\frac{\partial}{\partial t}\right)E\Big|_{x=0}=0. \tag{2.12}$$

To implement (2.12), we must approximate the derivatives by finite differences. One should follow two rules in approximating continuous ABCs by their finite difference equivalents. First, since the Yee FDTD algorithm is second-order accurate, we should use centered differences to maintain second-order accuracy in the ABCs. Furthermore, centered differences tend to result in more stable absorbing boundaries. Second, to maximize the stability of the boundary condition one should choose one point in space and time and ensure that all the factors in the finite-differenced ABC are centered on this one point, even if this means averaging some fields. The first-order Mur ABC for the x = 0 boundary is obtained

by finite-differencing (2.12) around a point one-half space step in from the boundary, and half a time step behind the time step currently being computed. By solving for the current field on the boundary, one obtains

$$E_0^n = E_1^{n-1} + \frac{c\Delta t - \Delta x}{c\Delta t + \Delta x}\left(E_1^n - E_0^{n-1}\right) \tag{2.13}$$

where superscripts and subscripts denote the time step and x index, respectively.

The second-order Mur ABC, which is found by taking the first two terms in the Taylor series expansion of the square root in (2.10) and multiplying through by $\partial/\partial t$ to clear the denominator, is

$$\left(\frac{1}{c}\frac{\partial^2}{\partial x \partial t} - \frac{1}{c^2}\frac{\partial^2}{\partial t^2} + \frac{1}{2}\left(\frac{\partial^2}{\partial y^2} + \frac{\partial^2}{\partial z^2}\right)\right)E\Big|_{x=0} = 0. \tag{2.14}$$

By approximating the derivatives in (2.14) by finite differences, one obtains a formula similar to, but more complicated than (2.13). Since the first- and second-order Mur boundary conditions are the ABCs most used for FDTD analysis by the EM community, they will often be used as a reference against which the other boundary conditions of Chapters 3 and 4 will be compared.

2.4 Other Free-Space Absorbing Boundary Conditions

There are two powerful ABCs which were not tested in this thesis. Lindman [5] develops an ABC by approximating the one-way wave equation in a manner different from that of Mur. An excellent discussion of this ABC is given by Chew [6]. However, Lindman's approach results in the introduction of auxiliary variables which must be finite-differenced in tandem with the field quantities of interest at points on the boundaries. This increases the computation required to implement the ABC somewhat, but more importantly adds a considerable amount of extra complexity to a program. Consequently, this ABC has never been widely used by the EM community. These auxiliary variables are basically used to find an estimate of the direction of propagation of waves, which in a guided-wave problem is known a priori. Furthermore, the boundary condition is designed to find the direction of

propagation of unguided waves via tangential derivatives; consequently, in a guided-wave problem it will suffer from the same difficulties, discussed in Chapter 3, which make the second-order Mur boundary condition inappropriate on the end walls. Lindman discusses an extension of the boundary condition which would allow it to absorb evanescent waves. However, this modified boundary condition appears to require that the Fourier components of the fields in the directions tangential to the boundary be known. Since this is not the case in the FDTD analysis of microstrip, this boundary condition appears inappropriate for the side walls as well.

Liao's boundary condition [7,6] also produces excellent absorption for free-space wave propagation problems. This boundary condition is also not used as extensively by the EM community as the Mur boundary conditions, primarily because it often becomes unstable. Since this boundary condition is for the absorption of traveling waves, it is not suitable for the side walls of a microstrip simulation, which are considered in Chapter 4. However, since Liao's ABC does not involve tangential derivatives, but tries to absorb waves based only on information normal to the boundary, this ABC may produce good results on the end walls of microstrip. The experience of other researchers has shown that the stability problems of this ABC are exacerbated by having a dielectric interface intersect the boundary, as is the case in the FDTD simulation of microstrip. Some work has been done on stabilizing the Liao ABC [8], however, and although this thesis does not test the performance of Liao's ABC on the microstrip end walls, this may be a fruitful direction for further research.

CHAPTER 3

BOUNDARY CONDITIONS TO ABSORB DISPERSIVE, GUIDED WAVES

The boundary conditions used to terminate many types of waveguiding structures in the longitudinal, or guiding, direction must be capable of absorbing waves which differ significantly from those typical in scattering problems. Instead of waves propagating in all directions in free space, one has waves which are guided and, hence, normally incident on the boundary. Since most waveguiding structures of practical interest are dispersive, and since FDTD analysis generally uses a broadband excitation, these guided waves will be traveling with a considerable range of velocities. This chapter describes several different absorbing boundary conditions, evaluates their applicability to the guided-wave problem on theoretical grounds, and tests their performance via the FDTD simulation of a uniform microstrip line. The discussion focuses on microstrip structures, since they are of the greatest commercial importance, but most of the conclusions are valid for any dispersive waveguiding structure. When boundaries contain adjustable input parameters, sensitivity studies are performed and guidelines for choosing these parameters intelligently are listed. Finally, this chapter summarizes the performance of the various ABCs and computes the frequency-dependent effective dielectric constant, $\varepsilon_{r,eff}$, of a uniform microstrip to illustrate how small reflections from ABCs in the time domain can lead to large errors in computed frequency domain quantities. Much of this chapter has previously been summarized in a paper by Betz and Mittra [9].

3.1 Description of Uniform Microstrip Test of ABCs

Most of this chapter involves individually describing and testing the ABCs implemented. The test used for this purpose is a uniform microstrip with a relative dielectric constant, ε_r, of 10.2, a dielectric thickness, H, of 2.54 mm, and a conductor width, W, of 2.54

mm. The geometry is discretized with a space step of 0.3175 mm in all three coordinate directions, and the time step is chosen to be 0.99 times the Courant stability limit, or 6.053 x 10^{-13} seconds. The geometry is excited on the z = 0 plane by the quasi-static field distribution of a microstrip, which is found via a finite-difference Laplace solver. The time variation of this excitation is a signal which is Gaussian with a 3 dB frequency of 8 GHz. The FDTD computational domain is 24Δx by 22Δy by 270Δz, and is shown graphically in Figure 3.1 (all figures appear at end of chapter).

A perfect magnetic conductor is used as a symmetry condition on the x = 0 boundary so that only half the geometry has to be modeled. The y = 0 boundary is a perfect electric conductor to model the microstrip ground plane, and the z = 0 boundary is a perfect electric conductor so that all the excitation energy propagates forward. The other three walls are made absorbing boundaries -- the second-order Mur boundary condition is enforced on the x = 24Δx and y = 22Δy walls, while the boundary condition to be tested is enforced on the end wall at z = 270Δz. Finally, the reflection caused by each of the different ABCs enforced on the end walls is found by monitoring the voltage under the microstrip conductor at the z = 250Δz plane and comparing it with the waveform obtained when the microstrip is 500 cells long in the z-direction. The larger problem will have no reflection from the z = 500Δz wall in the time interval of interest, so by subtracting the voltage waveforms obtained in the two simulations one finds the reflection introduced by the absorbing boundary condition on the end wall.

3.2 The First-Order Mur ABC

The derivation of this boundary condition was discussed in detail in Chapter 2. The first-order Mur boundary condition is the ABC most commonly used by the EM community to terminate FDTD analyses of guided-wave structures, largely because it is well-known and fairly simple to implement. The first-order Mur boundary condition is the discretized version of

$$\left(\frac{\partial}{\partial z}+\frac{1}{v}\frac{\partial}{\partial t}\right)E\Big|_{z=z_{max}}=0 \tag{3.1}$$

where v is the assumed normal velocity of the incident waves. Let us find the reflection this boundary would produce if the discretization introduced no additional error. Consider an incident guided wave of the form

$$E_{inc}(z,t)=e^{j\left(\omega t-\frac{\omega}{c}z\right)}. \tag{3.2}$$

where c is the normal component of the velocity of the incident waves. For boundary conditions which do not involve tangential derivatives the field variation in the tangential (x and y) directions is unimportant, so it has been omitted in (3.2). The total field at the boundary consists of the incident field plus whatever reflected field is necessary to satisfy the boundary condition. The incident and reflected fields are of the same mode, and hence travel at the same speed, so the total field is

$$E_{tot}(z,t)=e^{j\left(\omega t-\frac{\omega}{c}z\right)}+Re^{j\left(\omega t+\frac{\omega}{c}z\right)} \tag{3.3}$$

where R is the reflection coefficient of the boundary. Substituting this into the first-order Mur ABC formula, (3.1), yields

$$\left(-j\frac{\omega}{c}+j\frac{\omega}{v}\right)e^{j\left(\omega t-\frac{\omega}{c}z_{max}\right)}+R\left(j\frac{\omega}{c}+j\frac{\omega}{v}\right)e^{j\left(\omega t+\frac{\omega}{c}z_{max}\right)}=0. \tag{3.4}$$

By solving for R and ignoring the relative phase factor, one obtains

$$R=-\frac{(j\omega)(c-v)}{(j\omega)(c+v)}. \tag{3.5}$$

Two comments about this relation are in order. First, if the assumed speed of the wave, v, is the same as the true speed of the wave, c, there is no reflection. The greater the difference between the assumed and true speeds of the wave, the greater the reflection. Second, recall that this expression for the reflection has been derived under the assumption that the discretization introduces no additional error. In practice, the discretization will introduce some additional error, but so long as the discretization is reasonably fine, the

reflection coefficient will usually be close to that predicted by a continuous domain analysis. The exception tends to occur near $\omega = 0$. In the continuous domain this causes no problems -- the $j\omega$ terms in the numerator and denominator cancel exactly. In the discretized version of (3.1), however, the continuous derivatives are replaced by finite differences and reflection coefficients of zero over zero can tend to different numbers, depending on exactly how these finite differences are implemented, what the machine precision is, and several other factors. In the first-order Mur boundary condition the ABC tends to behave well near $\omega = 0$ [10,11], but as succeeding sections will point out, some higher-order boundary conditions have difficulty with the dc component of a signal.

In order to apply (3.1), one must choose a value for v, the assumed velocity of the incident wave. To assess the sensitivity of the first-order Mur boundary condition to this parameter, a uniform microstrip similar to that described in Section 3.1 was simulated with several different values of v used in the first-order Mur ABC terminating the line. In these tests v was set to one value over the entire end of the microstrip -- physically the normal velocities of the wave in the air and dielectric are the same, and the boundary condition parameters are set accordingly. Figure 3.2 shows how the energy in the reflected waveform varies as $\varepsilon_{r,eff}$ is varied, where $v = c_o/\sqrt{\varepsilon_{r,eff}}$ and c_0 is the speed of light in free space.

Figure 3.2 indicates that the first-order Mur ABC which assumes a uniform wave speed performs best for this problem when $\varepsilon_{r,eff}$ is assumed to be about 8.3. Recall that our excitation is Gaussian in time; hence its spectrum also has a Gaussian distribution. Furthermore, because we chose the 3 dB frequency to be 8 GHz, most of the signal energy lies below 8 GHz, and there is very little energy above 16 GHz. From formulae given by Gupta et al. [12], one finds that the quasi-static value of $\varepsilon_{r,eff}$ is approximately 6.99, the value at 8 GHz is about 8.73, and the value at 16 GHz is near 9.64. Since more energy lies between 0 and 8 GHz than above 8 GHz, equation (3.5) leads one to expect that choosing v in the ABC to perfectly absorb a wave at a frequency slightly less than 8 GHz would result in

the best overall absorption of the wideband signal. Consequently, the fact that the performance of the ABC is best when one chooses $\varepsilon_{r,eff}$ to be 8.3 is quite understandable.

There is an alternative way to implement the first-order Mur boundary condition on the end walls of microstrip line. Instead of assuming that the wave travels with one normal velocity, v, along the entire boundary, one chooses v to be the speed of light in air and the speed of light in the dielectric in the cells adjoining air and dielectric, respectively. One hopes that the overall effect of this ABC is to efficiently absorb guided waves which extend through both the air and dielectric, and whose speed is somewhere between the speeds of light in air and dielectric. Figure 3.3 compares the reflection produced by these two implementations of the first-order Mur ABC. Note that the ABC which assumes that the wave travels with the same speed over the entire boundary chooses v by assuming $\varepsilon_{r,eff}$ is 8.3, which, according to Figure 3.2, is optimal.

Figure 3.3 shows that the two implementations of the first-order Mur ABC produce about the same amount of reflection for a broadband excitation. For a narrow-band excitation, (3.5) suggests the single-speed ABC will perform better. Since the single-speed ABC requires an intelligent choice of the velocity of the guided waves, while the dual-speed ABC requires only that the material parameters of the microstrip be known, the dual-speed ABC is probably the boundary condition of choice for wideband excitations.

The reflection coefficient versus frequency plot in Figure 3.3(b) shows four local minima for the single-speed ABC. However, Equation (3.5), coupled with the fact that $\varepsilon_{r,eff}$ increases uniformly with frequency and hence the wave speed decreases uniformly with frequency, suggests that this plot should have only one local minimum; i.e., the plot should have a "v" shape. There are two reasons for the other local minima. First, the reflected waveform is monitored only out to 2500 time steps; after this multiple reflections will start to pollute the reflected waveform. This windowing in time corresponds to convolving the spectrum of the reflected wave with a sinc function, which will introduce some spurious

features in the reflection coefficient plot. Second, Equation (3.5) is based on a continuous-domain analysis; the discretization will cause some change in the reflection coefficient.

3.3 The Second-Order Mur ABC

The second-order Mur boundary condition was described in Section 2.3. The wave speed, c, of (2.14) is set to the speed of light in air and in dielectric in the regions of the boundary adjoining air and dielectric, respectively. Figure 3.4 shows its performance when it is applied to the uniform microstrip described in Section 3.1.

Clearly the second-order Mur ABC is not suitable for terminating the end walls of a microstrip structure, as it is approximately 30 times more reflective than a first-order Mur boundary. The tangential derivatives in (2.14) become undefined as one crosses the dielectric and conductor boundaries which form the microstrip, and therefore act as a source for the reflected wave. Some readers may be concerned by the fact that the reflection coefficient of this ABC is greater than one for low frequencies. This is, however, perfectly legitimate; an ABC is a source of a reflected wave, not a passive component, so the reflection coefficient can be greater than one. In fact, many absorbing boundary conditions can become unstable, and in this case their reflection coefficients approach infinity.

Since it is the tangential derivatives in the second-order Mur ABC which make it so poorly suited to the termination of the guided-wave ends of microstrip, one may ask if these tangential derivatives can be converted to normal derivatives. Indeed they can. The equation defining a second-order Mur ABC on the $z = z_{max}$ wall is

$$\left(\frac{1}{c}\frac{\partial^2}{\partial z \partial t}+\frac{1}{c^2}\frac{\partial^2}{\partial t^2}-\frac{1}{2}\left(\frac{\partial^2}{\partial x^2}+\frac{\partial^2}{\partial y^2}\right)\right)E\Big|_{z=z_{max}} = 0. \tag{3.6}$$

From the wave equation, (2.1), one finds that

$$\frac{1}{2}\left(\frac{\partial^2 E}{\partial x^2}+\frac{\partial^2 E}{\partial y^2}\right)=\frac{1}{2c^2}\frac{\partial^2 E}{\partial t^2}-\frac{1}{2}\frac{\partial^2 E}{\partial z^2}. \tag{3.7}$$

Equation (3.7) can be used to eliminate the tangential derivatives from (3.6); the new boundary condition is

$$\left(\frac{1}{c}\frac{\partial^2}{\partial z \partial t}+\frac{1}{2c^2}\frac{\partial^2}{\partial t^2}+\frac{1}{2}\frac{\partial^2}{\partial z^2}\right)E|_{z=z_{max}} = 0. \tag{3.8}$$

Multiplying by 2 and factoring yield

$$\left(\frac{\partial}{\partial z}+\frac{1}{c}\frac{\partial}{\partial t}\right)\left(\frac{\partial}{\partial z}+\frac{1}{c}\frac{\partial}{\partial t}\right)E|_{z=z_{max}} = 0. \tag{3.9}$$

This ABC is simply a special case of the dispersive boundary condition discussed in the next section in which the two speeds, v_1 and v_2, are chosen to be equal and are represented by c.

3.4 Litva's Dispersive Boundary Condition

Higdon [10,13] has developed a boundary condition to absorb waves incident from various angles on a boundary in a scattering-type problem. The parameters input to the boundary condition are the speeds divided by the angles of incidence, $c/\cos(\theta)$, of the incident waves. Bi et al. [14] showed that one could use this boundary condition to terminate the ends of microstrip lines if one interpreted the $c/\cos(\theta)$ factors as the normal velocities of incident waves. The dispersive boundary condition enforces

$$\left(\frac{\partial}{\partial z}+\frac{1}{v_1}\frac{\partial}{\partial t}\right)\left(\frac{\partial}{\partial z}+\frac{1}{v_2}\frac{\partial}{\partial t}\right)E|_{z=z_{max}} = 0. \tag{3.10}$$

Notice that this boundary condition looks like two first-order Mur boundary conditions superposed. Since the two factors are designed to absorb waves perfectly at two different incident speeds, one would expect this ABC to be a better absorber of broadband signals on a dispersive structure than the first-order Mur boundary condition. By discretizing (3.10) via centered differences about a point Δz into the mesh and Δt back in time from the boundary point being updated, one obtains the update equation

$$E_M^n = 2E_{M-1}^{n-1} - E_{M-2}^{n-2} + (\gamma_1+\gamma_2)\left(E_M^{n-1} - E_{M-1}^n - E_{M-1}^{n-2} + E_{M-2}^{n-1}\right) - \gamma_1\gamma_2\left(E_M^{n-2} - 2E_{M-1}^{n-1} + E_{M-2}^n\right) \tag{3.11}$$

where subscripts and superscripts denote the z index and the time step, respectively, and

$$\gamma_i = \frac{1-\rho_i}{1+\rho_i}, \qquad \rho_i = \frac{v_i \Delta t}{\Delta z}. \tag{3.12}$$

We can find the reflection that the continuous boundary condition, (3.10), would generate by repeating the procedure outlined in Section 3.2. Assume an incident field of the form (3.2); then the total field will be of the form given by (3.3). Substituting this field into (3.10) yields

$$\begin{aligned} &\left(-j\frac{\omega}{c}+j\frac{\omega}{v_1}\right)\left(-j\frac{\omega}{c}+j\frac{\omega}{v_2}\right)e^{j\left(\omega t-\frac{\omega}{c}z_{max}\right)} \\ &+R\left(j\frac{\omega}{c}+j\frac{\omega}{v_1}\right)\left(j\frac{\omega}{c}+j\frac{\omega}{v_2}\right)e^{j\left(\omega t+\frac{\omega}{c}z_{max}\right)}=0. \end{aligned} \tag{3.13}$$

This can immediately be solved for the reflection coefficient, R, which, neglecting the relative phase factor, is given by

$$R = -\frac{(j\omega)^2(c-v_1)(c-v_2)}{(j\omega)^2(c+v_1)(c+v_2)}. \tag{3.14}$$

Since each (c-v) / (c+v) factor is always less than one, (3.14) implies that this boundary condition should perform better than the first-order Mur boundary condition. To see if this is the case, the uniform microstrip described in Section 3.1 was simulated, and the reflection data thus obtained are displayed in Figure 3.5.

The dispersive boundary condition (DBC) performs well for most frequencies, with a reflection coefficient which is smaller than that of a first-order Mur, but near dc this boundary condition becomes quite reflective. Figure 3.5(a) shows that the reflected wave has a dc component which does not appear to decay. Therefore, if one monitored the reflection for all time, one would find that the reflection coefficient at dc is an impulse. Clearly this is unacceptable; all of our low-frequency data will be polluted.

The reflection coefficient predicted by (3.14) contains a $(j\omega)^2/(j\omega)^2$ term, which at dc becomes zero over zero. While this presents no difficulties in the continuous domain, when discretized the numerator and denominator may not approach zero at the same speed, and we

may obtain a large dc reflection. The higher the order of the boundary condition, the greater the power of jω in (3.14) and the more problematic the dc behavior of a boundary condition. In fact, for boundary conditions of higher order than (3.10), the boundary condition often becomes unstable and generates errors which completely swamp the solution. Whether or not the second-order DBC, (3.10), generates spurious dc signals depends on many subtle factors: the exact order of additions in the boundary update equations, the spatial distribution of the incident field, and the boundary conditions applied to the other walls terminating the computational domain [11]. The DBC has always had difficulty near dc in the FDTD code used in this work; other researchers, with slightly different codes, report that sometimes the DBC works properly and sometimes it does not. Clearly this is unacceptable; a boundary condition which, at best, works fifty percent of the time is of little utility.

3.5 A Modified Dispersive Boundary Condition

In order to improve the performance of the dispersive boundary condition near dc, we add a damping term, α_1, to one of the two factors:

$$\left(\frac{\partial}{\partial z}+\frac{1}{v_1}\frac{\partial}{\partial t}+\alpha_1\right)\left(\frac{\partial}{\partial z}+\frac{1}{v_2}\frac{\partial}{\partial t}\right)E\Big|_{z=z_{max}}=0. \tag{3.15}$$

In discretized form on the $z = z_{max} = M\Delta z$ boundary this becomes

$$\begin{aligned} E_M^n = {} & (\beta+1)E_{M-1}^{n-1}-\beta E_{m-2}^{n-2}-\gamma_1\gamma_2(E_M^{n-2}-2E_{M-1}^{n-1}+E_{M-2}^n) \\ & -(\beta\gamma_2+\gamma_1)(E_{M-1}^{n-2}-E_{M-2}^{n-1})+(\gamma_1+\gamma_2)(E_M^{n-1}-E_{M-1}^n) \end{aligned} \tag{3.16}$$

where superscripts denote the time step, subscripts denote the z index and

$$\rho_i=\frac{v_i\Delta t}{\Delta z} \qquad \gamma_i=\frac{1-\rho_i}{1+\rho_i(1+\alpha_i\Delta z)} \qquad \beta=\frac{1+\rho_1}{1+\rho_1(1+\alpha_1\Delta z)}. \tag{3.17}$$

Note that α_2 is implicitly zero in the formula for γ_1. Adding damping terms to both factors in (3.15) rather than to only one degrades the boundary condition's performance. Only one damping term is necessary to stabilize the dc behavior of the DBC, and since damping terms adversely affect the DBC's performance at other frequencies, one should use only one.

Once again, we will apply the procedure outlined in Section 3.2 to find the reflection coefficient of the continuous boundary condition. Substitute a wave of the form (3.3) into (3.15) to obtain

$$\left(-j\frac{\omega}{c}+j\frac{\omega}{v_1}+\alpha_1\right)\left(-j\frac{\omega}{c}+j\frac{\omega}{v_2}\right)e^{j\left(\omega t-\frac{\omega}{c}z_{max}\right)} + R\left(j\frac{\omega}{c}+j\frac{\omega}{v_1}+\alpha_1\right)\left(j\frac{\omega}{c}+j\frac{\omega}{v_2}\right)e^{j\left(\omega t+\frac{\omega}{c}z_{max}\right)}=0. \tag{3.18}$$

One can then solve for R,

$$R=-\frac{(j\omega)(j\omega c-j\omega v_1+\alpha_1 c v_1)(c-v_2)}{(j\omega)(j\omega c+j\omega v_1+\alpha_1 c v_1)(c+v_2)}, \tag{3.19}$$

where the relative phase factor has been ignored. Note that the power of the $j\omega/j\omega$ factor in Equation (3.19) has been reduced from two to one. By letting ω approach zero, we see that the reflection near dc should be the same as that from a first-order Mur ABC with assumed incident velocity v_2. Equation (3.19) suggests that one should choose α_1 to be as small as possible in order to minimize the reflection. However, α_1 must still be large enough to stabilize the behavior of the DBC. Comparison of Equations (3.17) and (3.12) shows that the update equations for the discretized boundary condition are changed by the addition of several $\alpha_1\Delta z$ terms. This suggests that one should choose α_1 in relation to Δz, i.e. $\alpha_1 = k/\Delta z$, in order to change the update equations sufficiently to stabilize this ABC's dc behavior while not ruining its high-frequency performance.

An important question is how sensitive this modified dispersive boundary condition is to its input parameters. Figure 3.6 shows the dependence of the reflected energy on the choice of α_1, while Figure 3.7 indicates the relationship between reflected energy and the two wave-speed parameters, v_1 and v_2.

One can see from Figure 3.6 that the modified DBC using any value of α_1 between $0.02/\Delta z$ and $0.25/\Delta z$ yields better performance than a first-order Mur boundary condition, while a value of about $0.05/\Delta z$ appears to be optimal. One should choose α_1 to be greater

than about $0.02/\Delta z$ to ensure the dc problems of the DBC are corrected. From Figure 3.7 we see that the reflection coefficient is considerably less sensitive to $\varepsilon_{r,eff1}$ than it is to $\varepsilon_{r,eff2}$. This behavior can be understood from the form of Equation (3.19); the attenuation term, α_1, in the first factor tends to reduce the sensitivity of the boundary condition to v_1. For the microstrip simulated in Figure 3.7, the optimal values of $\varepsilon_{r,eff1}$ and $\varepsilon_{r,eff2}$ are about 7 and 9, respectively. In general, then, one should choose α_1 to be about $0.05/\Delta z$, $\varepsilon_{r,eff1}$ to be near the quasi-static value and $\varepsilon_{r,eff2}$ to be near the value at the high-frequency end of the excitation.

Figure 3.8 compares the performance of this modified DBC with that of a first-order Mur boundary condition when they are used to terminate the microstrip of Section 3.1. The modified DBC clearly performs better than a first-order Mur boundary. Figure 3.8(a) shows that the time-domain reflection is smaller than that from a first-order Mur, and that there is no dc signal being generated. Figure 3.8(b) shows that the modified DBC has a lower reflection coefficient than the first-order Mur ABC over almost all of the frequency band of interest. The very large dc reflection coefficient of Litva's original DBC has been brought under control by the addition of the damping factor, α_1.

3.6 The Superabsorbing Boundary Algorithm

Fang and Mei [15] and Mei and Fang [16] have developed an algorithm which can be used to improve the performance of many ABCs. Typically in EM analysis, one applies an absorbing boundary condition to the tangential E-field nodes which lie on the boundary. Consider, for example, an absorbing boundary on the $z = z_{max}$ plane in a three-dimensional simulation. One uses this ABC to calculate the values of E_x and E_y. H_z also lies on the boundary, but it need not be calculated, since it never enters into the calculation of any of the interior nodes. Once E_x and E_y are known on the boundary, all the fields at all of the interior nodes can be found via the usual FDTD update equations [1]. Since there is some error in the ABC, the values of E_x and E_y on the boundary contain some error, and consequently when

H_x and H_y a half cell in are computed using these boundary values, they will also contain some error. The superabsorbing boundary algorithm begins by computing the H-fields a half cell into the mesh in two ways: via the ABC that was used to compute the E-fields on the boundary, and via the normal FDTD update equations. In [16] it is shown that the error in these two H-field values is of opposite sign and is related, so that a weighted average of these two H-field values can be used to cancel the leading-order errors in the boundary H-fields. For a boundary at the $z = M\Delta z$ plane the proper weighted average is

$$H_{M-1/2}^{n+1/2,final} = \frac{H_{M-1/2}^{n+1/2,curl} + \rho H_{M-1/2}^{n+1/2,ABC}}{1+\rho} \tag{3.20}$$

where the M-1/2 subscripts indicate that the H-fields are half a cell in from the $z = M\Delta z$ boundary and the n+1/2 superscripts indicate that the H-fields are half a time step ahead of the E-fields on the boundary. The words final, curl and ABC denote the corrected H-field, the H-field found via the usual discretized curl update equations, and the H-fields computed using the ABC, respectively. Finally, the weighting factor, ρ, is

$$\rho = \frac{c\Delta t}{\Delta z} \tag{3.21}$$

where c is the normal velocity of the incident waves.

The H-fields thus computed contain considerably less error than they would if they had been updated from the usual FDTD curl relations. However, the E-fields on the boundary still contain all the error introduced by the ABC; if this ABC uses previous values of the E-fields on the boundary to compute the E-fields at subsequent time steps, these boundary E-fields must be corrected. A derivation of these correction equations for three-dimensional problems is presented below.

Consider a boundary at the $z = M\Delta z$ plane. Ampere's Law states that

$$\nabla \times \overline{E} = -\mu \frac{\partial \overline{H}}{\partial t}. \tag{3.22}$$

Two components of this vector differential equation are

$$-\mu\frac{\partial H_x}{\partial t}=\frac{\partial E_z}{\partial y}-\frac{\partial E_y}{\partial z}$$
$$\mu\frac{\partial H_y}{\partial t}=\frac{\partial E_z}{\partial x}-\frac{\partial E_x}{\partial z}. \tag{3.23}$$

Discretizing these two equations via centered differences and solving for the desired fields on the boundaries yield

$$E_y^n(i,j-\tfrac{1}{2},k)=\frac{\mu\Delta z}{\Delta t}\left(H_x^{n+1/2}(i,j-\tfrac{1}{2},k-\tfrac{1}{2})-H_x^{n-1/2}(i,j-\tfrac{1}{2},k-\tfrac{1}{2})\right)$$
$$+E_y^n(i,j-\tfrac{1}{2},k-1)+\frac{\Delta z}{\Delta y}\left(E_z^n(i,j,k-\tfrac{1}{2})-E_z^n(i,j-1,k-\tfrac{1}{2})\right) \tag{3.24}$$

$$E_x^n(i-\tfrac{1}{2},j,k)=\frac{-\mu\Delta z}{\Delta t}\left(H_y^{n+1/2}(i-\tfrac{1}{2},j,k-\tfrac{1}{2})-H_y^{n-1/2}(i-\tfrac{1}{2},j,k-\tfrac{1}{2})\right)$$
$$+E_x^n(i-\tfrac{1}{2},j,k-1)+\frac{\Delta z}{\Delta x}\left(E_z^n(i,j,k-\tfrac{1}{2})-E_z^n(i-1,j,k-\tfrac{1}{2})\right) \tag{3.25}$$

where the notation (i,j,k) denotes the point in space with coordinates ($i\Delta x$, $j\Delta y$, $k\Delta z$).

In summary, then, implementing the superabsorbing boundary algorithm involves the following five steps:

1) apply an absorbing boundary condition to find the values of the tangential electric fields on the boundary;
2) use the same ABC to compute the tangential magnetic fields one-half cell in from the boundary and call these fields H^{ABC};
3) calculate the tangential magnetic fields one-half cell in from the boundary via the usual FDTD update equations and call these fields H^{curl};
4) find the more accurate values of the tangential magnetic fields one-half cell in from the boundary by averaging H^{curl} and H^{ABC} as specified by (3.20);
5) use (3.24) and (3.25) to recalculate the tangential electric fields on the boundary.

The superabsorbing boundary algorithm was applied to the two types of first-order Mur boundaries and to both the original and modified dispersive boundary conditions. The results are shown in Figures 3.9 and 3.10.

Clearly the superabsorbing boundary algorithm reduced the reflectivity of all four ABCs tested. However, it improved different ABCs by different amounts. Using the first norms of the reflection, one finds that the performance of the single-speed and dual-speed first-order Mur ABCs improved by factors of 5.6 and 3.0, respectively, while that of the original and modified DBCs improved by factors of 1.4 and 2.6, respectively. The fairly modest improvement in the absorption of the original DBC occurs because superabsorption does not cure this ABC's difficulty near dc. Superabsorption causes the greatest improvement when it is applied to the single-speed first-order Mur ABC because this boundary condition and the superabsorbing algorithm make the same assumptions about the behavior of the incident wave; both are designed to provide peak performance when a single plane wave is incident on the boundary. All of the four boundary conditions tested use previous values of the electric field on the boundary to predict subsequent values. Consequently, one should use Equations (3.24) and (3.25) to correct these fields as part of the superabsorbing algorithm, and this was done in the computations used to obtain Figures 3.9 and 3.10. Numerical experiments were also conducted in which the electric fields were not corrected -- only the magnetic field values were recomputed using superabsorption -- and it was found that this reduced the performance improvement due to superabsorption by about 50%.

The most effective boundary condition tested in this chapter was the single-speed first-order Mur ABC with superabsorption applied. Of course, then, we are interested in this ABC's sensitivity to the choice of wave speed, v, for the first-order Mur ABC and of c for the superabsorbing algorithm. It appears to be best to choose these two speeds to be the same; Figure 3.11 shows how the reflected energy varies as these speeds are changed.

Clearly the superabsorbing boundary algorithm not only improves the performance of the first-order Mur ABC; it also reduces its sensitivity to the assumed speed of the incident wave. For best results when using a first-order Mur ABC coupled with superabsorption, one should choose a value of $\varepsilon_{r,eff}$ which is quite high, typically only slightly below the substrate

relative dielectric constant. For example, the microstrip of Section 3.1 has a substrate ε_r of 10.2 and the optimal $\varepsilon_{r,eff}$ for use with this boundary condition is 9.6.

3.7 Summary of ABC Test Results

Table 3.1 lists all of the boundary conditions tested in this chapter starting with the ABC which offered the best performance for the termination of microstrip end walls, and ending with the least suitable ABC. Three measures of each ABC's performance are listed: the L_1, L_2, and L_∞ norms of the reflected signal. The definitions of these norms are given by Chen in [17]; the L_1, L_2, and L_∞ norms are the sum of the absolute values, the square root of the sum of the squares, and the maximum, respectively, of the time-sampled reflection signal.

In summary, then, the second-order Mur ABC is completely unsuitable for the termination of microstrip line simulations in the guiding direction. Litva's original DBC suffers from instability problems near dc that lead to poor absorption of low-frequency signal components. The modified DBC alleviates these dc problems and provides performance significantly better than that of a first-order Mur ABC. The superabsorbing boundary algorithm improves the performance of all the ABCs tested, and the best termination for the guiding end of a microstrip line is a single-speed first-order Mur ABC with superabsorption applied.

3.8 Effect of Guiding-End ABCs on the Calculation of ε_{eff}

The reflections generated by the various ABCs tested in the previous sections are quite small -- the peak of the reflected signal ranges from about 2.5% of the peak of the incident signal for the first-order Mur ABC to about 0.33% for the superabsorbing first-order Mur ABC. The reader may wonder, then, how important it is to use the more advanced ABCs presented in this chapter; perhaps 2.5% error is close enough. Unfortunately, an error of 2.5% in the time-domain waveforms can lead to significantly larger errors when this data

set is Fourier transformed and post-processed to yield frequency-domain parameters [18], which are usually the quantities of the greatest interest to circuit designers.

As an example, let us find the frequency-dependent effective dielectric constant, ε_{eff}, of the microstrip line described in Section 3.1. The microstrip modeled is exactly as described in Section 3.1; however, the size of the mesh surrounding it is changed. The side walls in the x- and y-directions are now both at 40Δ, where Δ is the space step in all directions, so that these walls will not cause large errors in the computation. The microstrip is 70Δ long in the z-direction, and the voltage under the center of the strip is monitored at $z = 20\Delta$ and $z = 65\Delta$. These results are compared with those from a microstrip which is 500Δ long in the z-direction, and which, therefore, should have no reflection from the end wall in the time interval simulated. Some authors use the average of the voltage computed at each point across the strip instead of the voltage at the strip center; both methods were tested and found to yield identical results, which indicates that voltage uniqueness is maintained well in the frequency range of interest.

$\varepsilon_{r,eff}$ is extracted from the time-domain data via the following procedure [18]. The voltages are Fourier transformed to the frequency domain,

$$\tilde{V}(\omega,z) = \int_{-\infty}^{\infty} V(t,z)e^{-j\omega t}dt. \tag{3.26}$$

To find the transfer function of a section of microstrip, we take the ratio of the voltage found at two different points along the line

$$e^{-\alpha(\omega)L-j\beta(\omega)L} = \frac{\tilde{V}(\omega,z_2)}{\tilde{V}(\omega,z_1)}. \tag{3.27}$$

Since the inverse of the complex exponential is multivalued, when one inverts (3.27) to find $\beta(\omega)$ one must use the facts that $\beta(0) = 0$ and β increases monotonically with ω in order to choose the correct value from the infinite number of possibilities. $\varepsilon_{r,eff}$ is related to β by

$$\beta(\omega) = \omega\sqrt{\mu_o\varepsilon_o\varepsilon_{r,eff}} \tag{3.28}$$

which implies

$$\varepsilon_{r,eff}(\omega)=\frac{\beta^2(\omega)}{\omega^2\varepsilon_o\mu_o}. \tag{3.29}$$

Figure 3.12 compares the $\varepsilon_{r,eff}$ curves computed using three different absorbing boundaries with the curve obtained using an extremely large computational domain and which therefore contains no reflection from the end wall. The quasi-static value of $\varepsilon_{r,eff}$ predicted by heuristic formulas [12], which is 7.0 in this case, is used to compute the wave-speed parameter of the single-speed first-order Mur ABC. This is the ABC most commonly used by the EM community today.

Clearly even the relatively small errors in the time domain caused by ABCs lead to significant errors in the $\varepsilon_{r,eff}$ curves. The curve computed with the superabsorbing ABC lies essentially on top of the reference curve, except for a small deviation near dc. Both first-order Mur ABCs introduce large, visible errors.

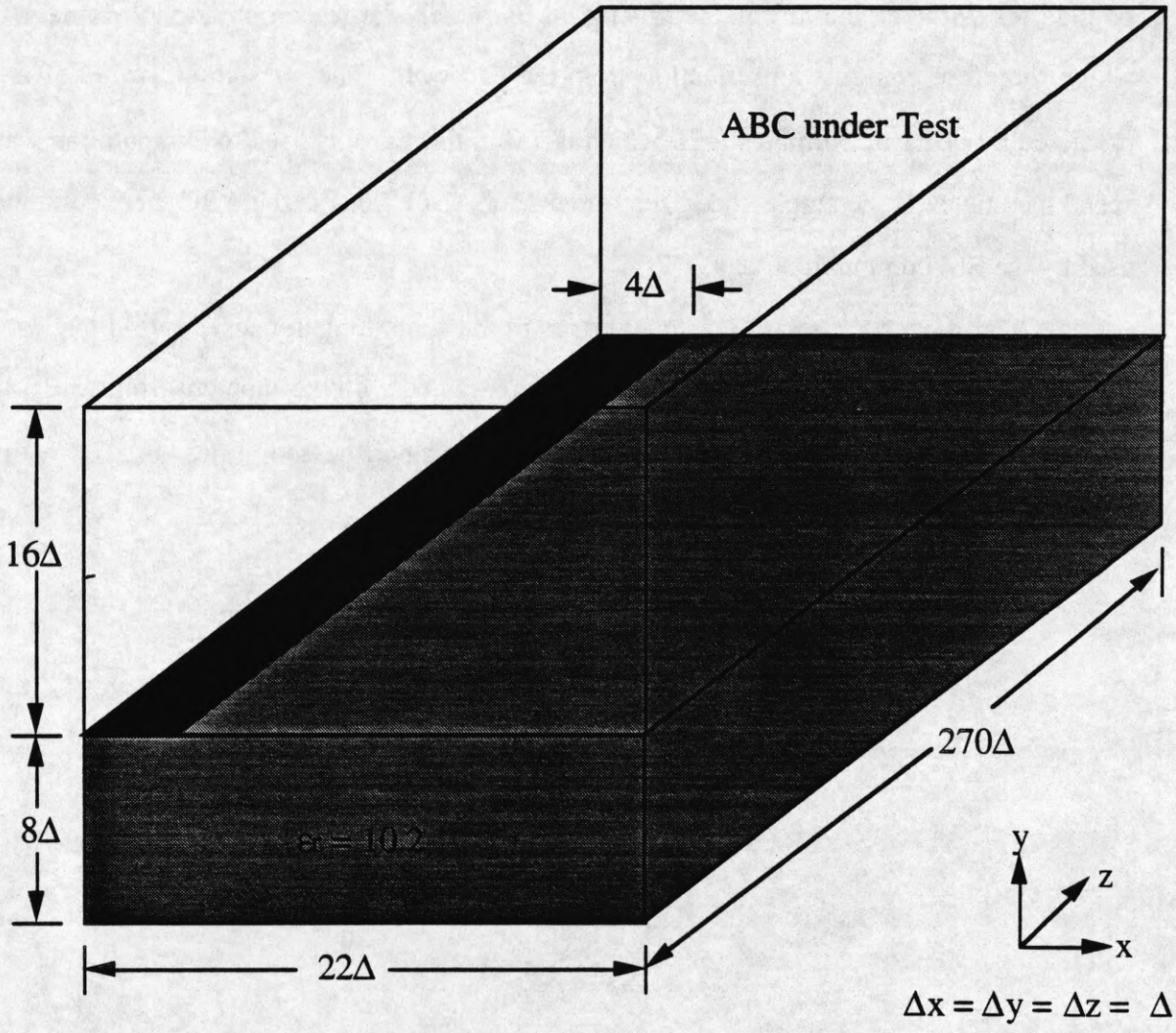

Figure 3.1 Uniform microstrip geometry used to evaluate the performance of various ABCs on the end walls.

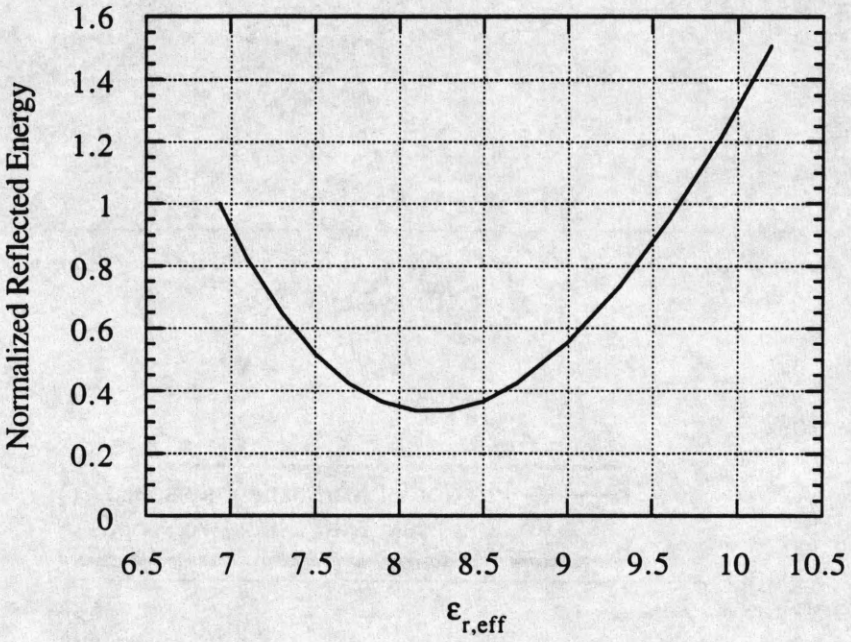

Figure 3.2 Variation of energy reflected by a first-order Mur ABC as $\varepsilon_{r,eff}$ is varied. The ABC assumes the wave speed, v, $= c_o/\sqrt{\varepsilon_{r,eff}}$. This graph was generated by simulating a microstrip identical to that described in Section 3.1, except that the conductor width, W, was 2.3 mm instead of 2.54 mm.

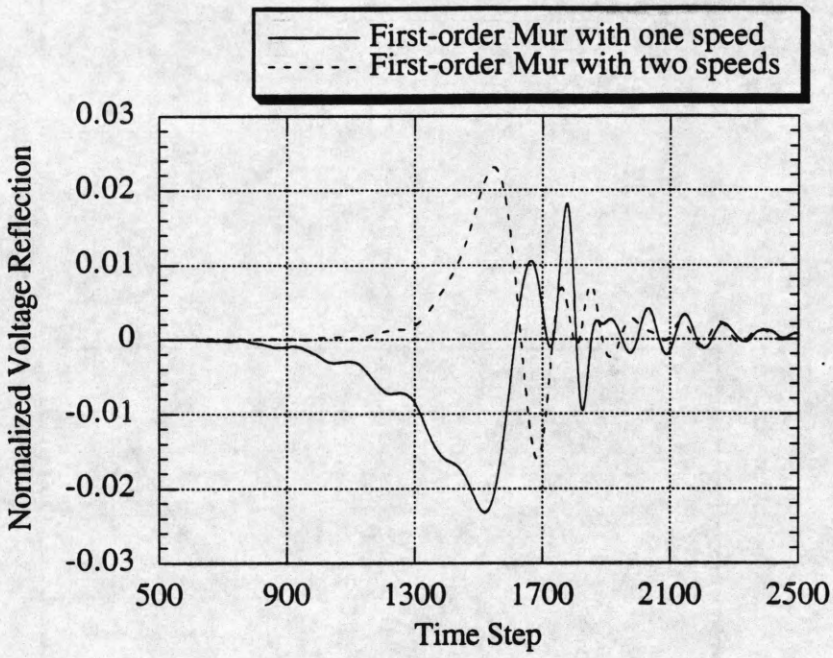

(a)

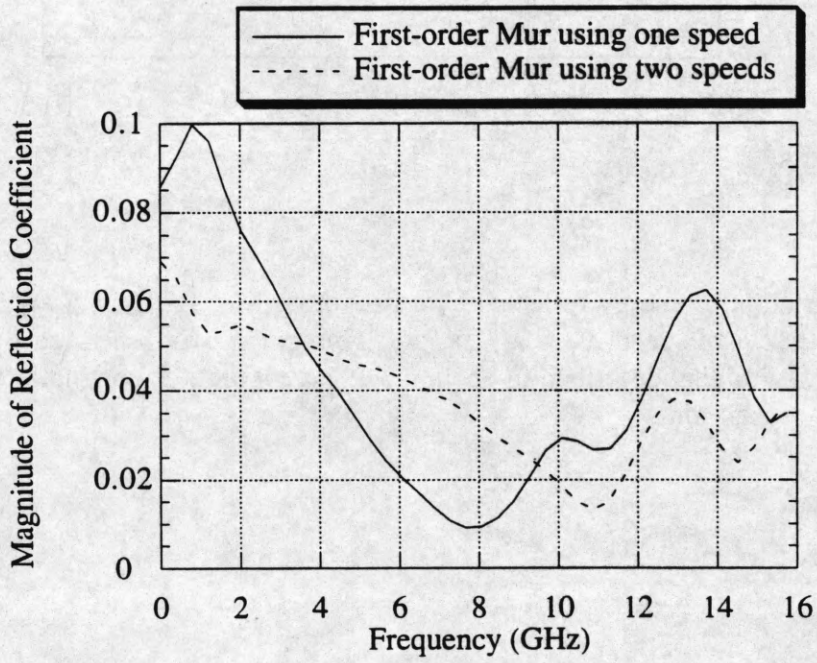

(b)

Figure 3.3 Comparison of reflections from two different types of first-order Mur ABCs in (a) the time domain and (b) the frequency domain. The one-speed Mur ABC calculates the speed, v, assuming $\varepsilon_{r,eff} = 8.3$.

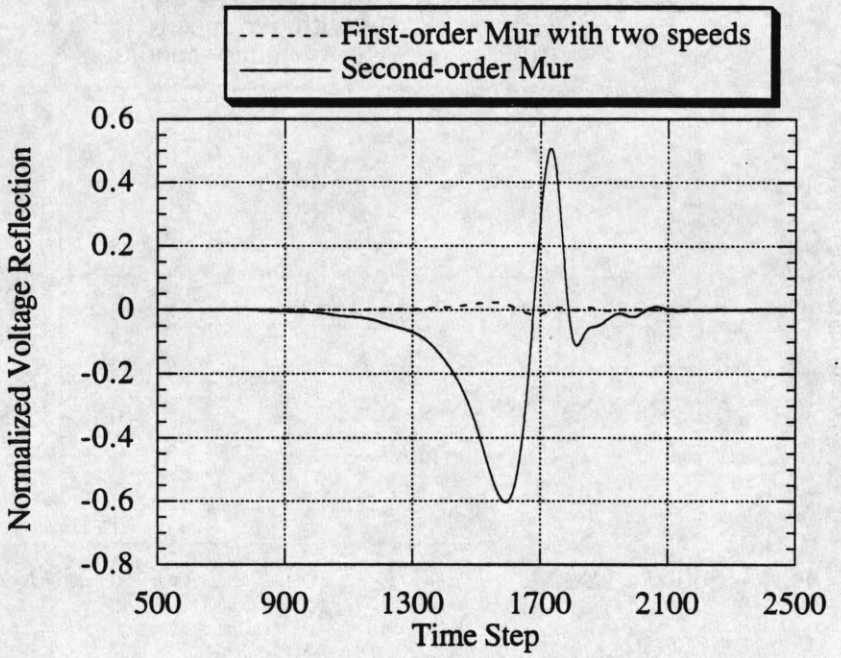

(a)

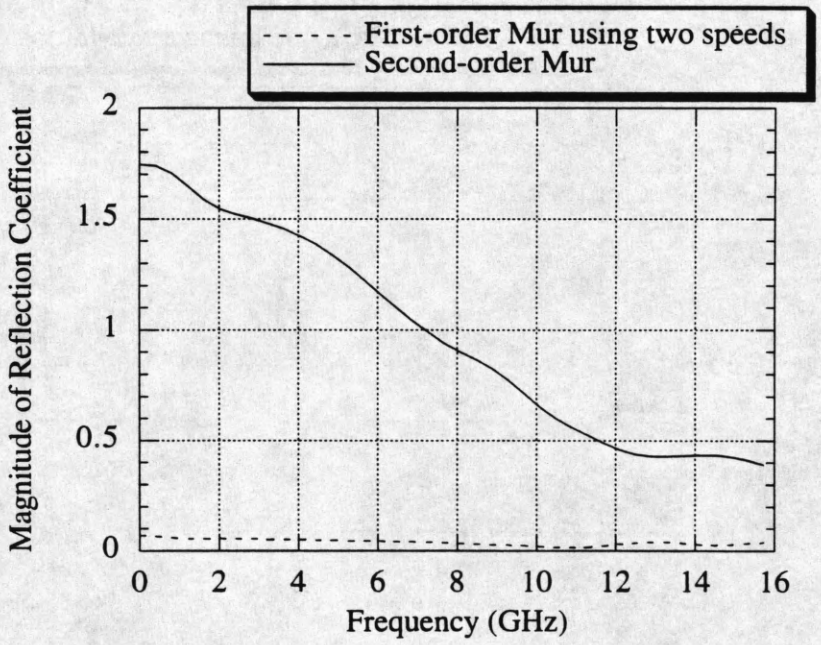

(b)

Figure 3.4 Reflection from a second-order Mur absorbing boundary in (a) the time domain and (b) the frequency domain.. The reflection from a first-order Mur ABC is shown for comparison.

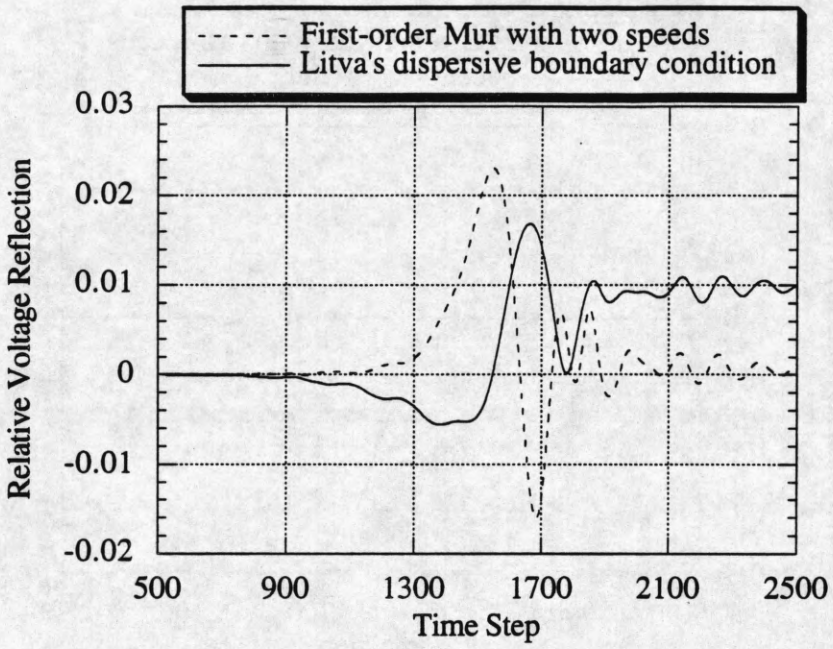

(a)

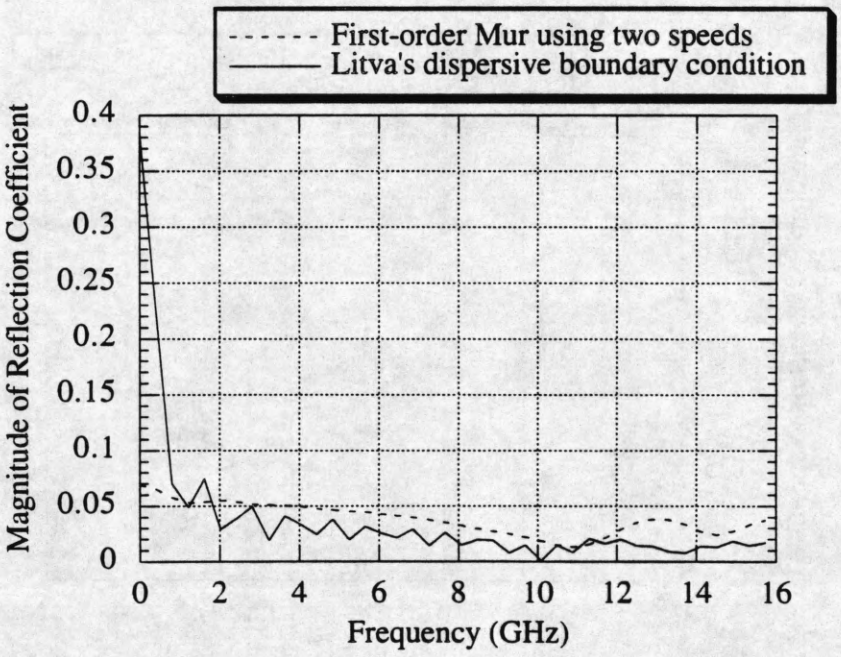

(b)

Figure 3.5 The (a) time-domain and (b) frequency-domain reflection from Litva's dispersive boundary condition compared to that of a first-order Mur boundary condition.

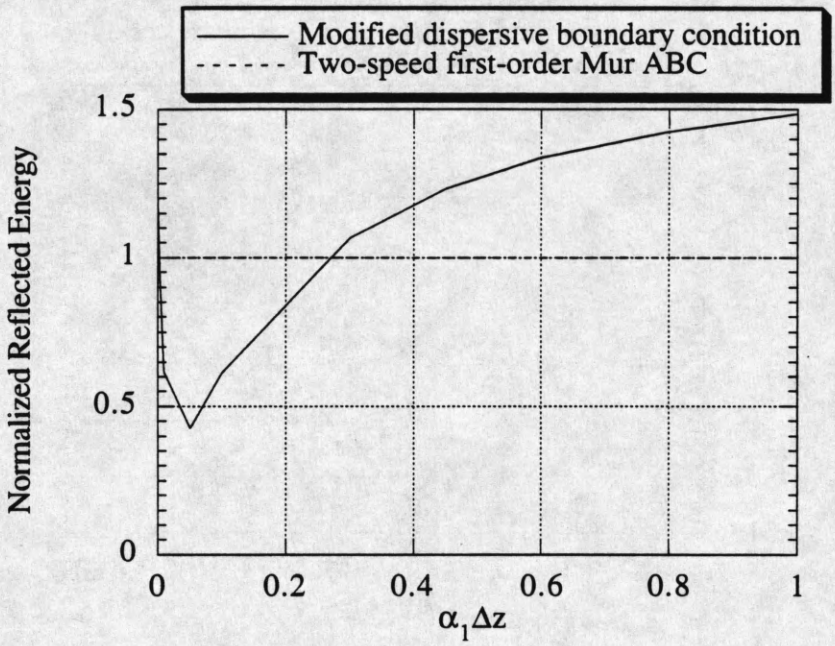

Figure 3.6 Dependence of reflected energy on the attenuation factor, α_1, in the modified dispersive boundary condition found via a uniform microstrip simulation. The microstrip simulated is described in Section 3.1, and the DBC uses $\varepsilon_{r,eff1} = 7.12$ and $\varepsilon_{r,eff2} = 8.50$.

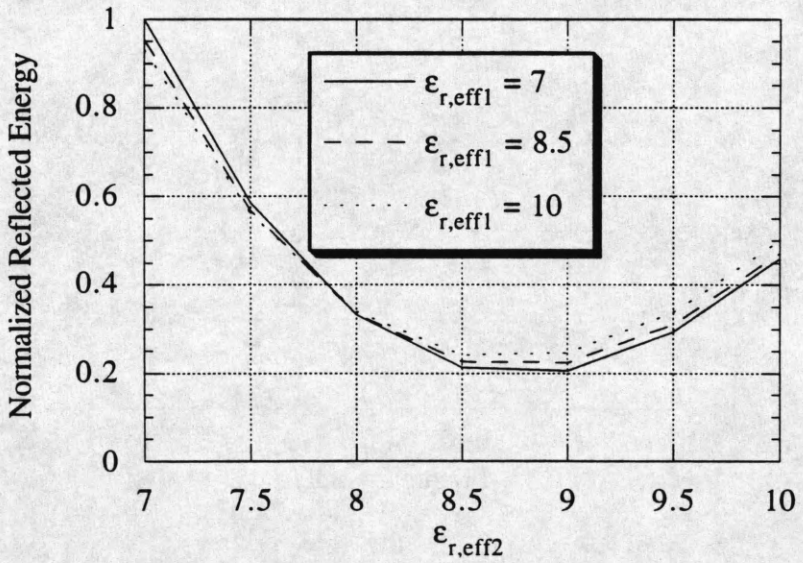

Figure 3.7 Relation between reflected energy and the wave speeds used in the modified dispersive boundary condition. The simulated microstrip differs slightly from that described in Section 3.1 in that W = 2.3 mm instead of 2.54 mm. The DBC uses $\alpha_1 = 0.1/\Delta z$ and the two wave-speed parameters are set according to $v_i = c_o / \sqrt{\varepsilon_{r,eff,i}}$.

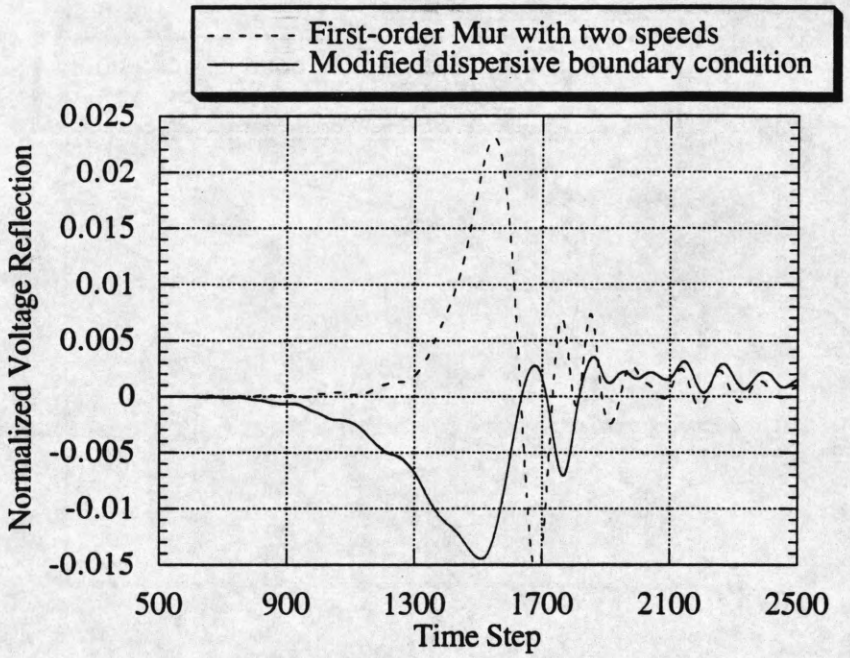

(a)

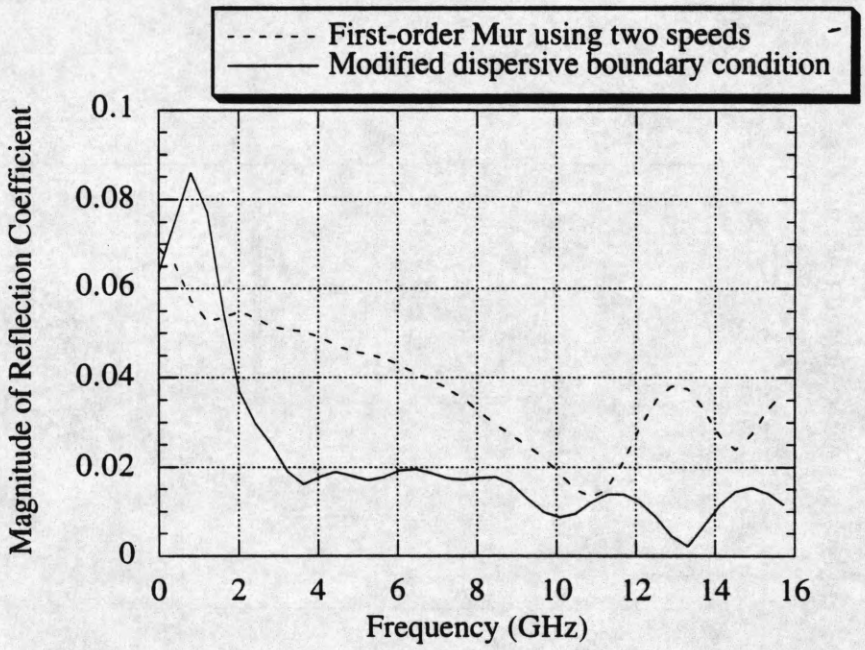

(b)

Figure 3.8 Reflection from a modified dispersive boundary condition in (a) the time domain and (b) the frequency domain compared with that from a first-order Mur ABC. The DBC parameters are $\alpha_1 = 0.1/\Delta z$, $\varepsilon_{r,eff1} = 7.12$, and $\varepsilon_{r,eff2} = 8.50$.

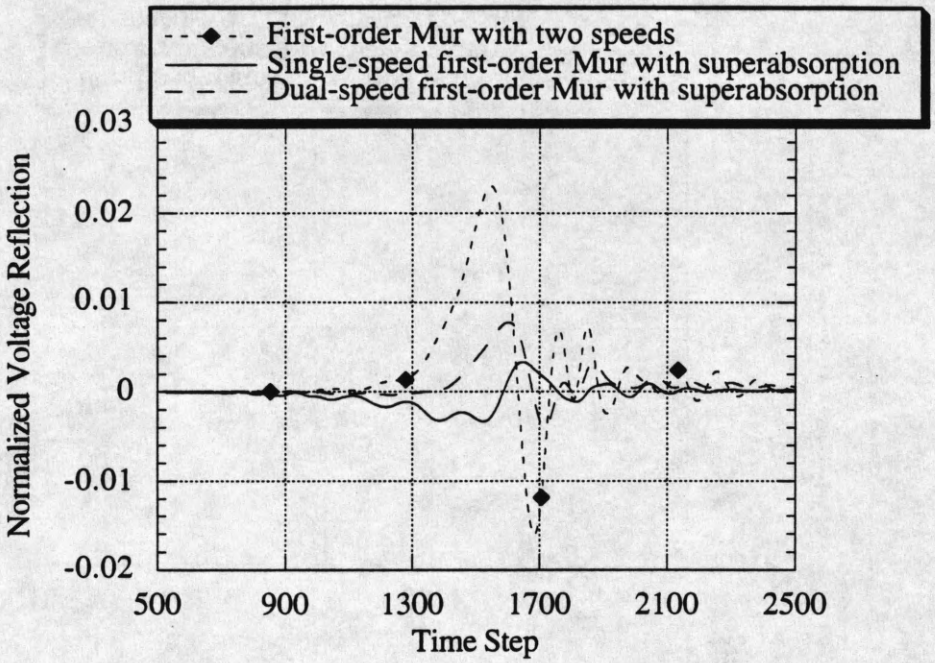

(a)

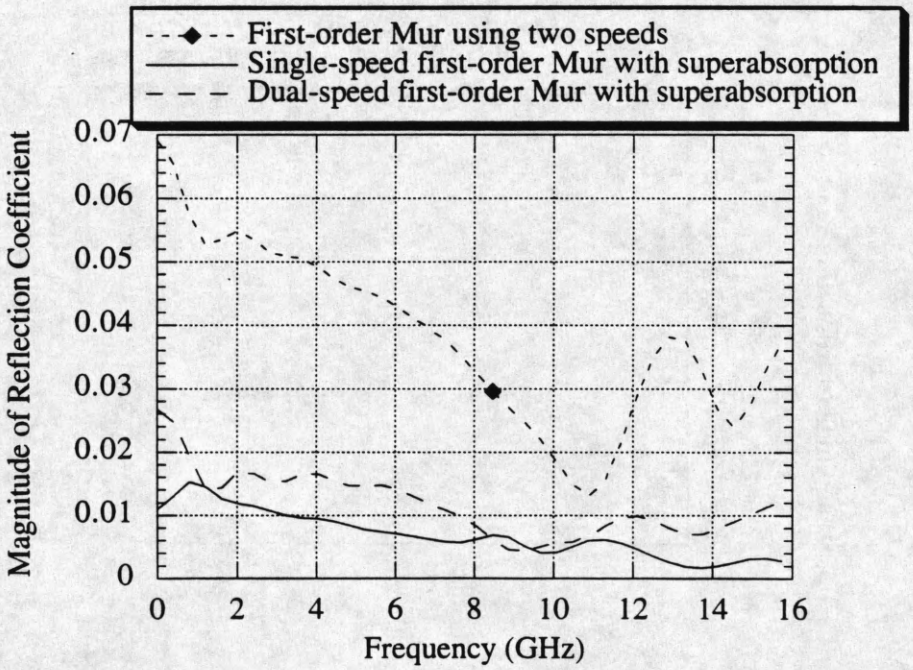

(b)

Figure 3.9 The (a) time-domain and (b) frequency-domain reflection from first-order Mur boundary conditions with and without superabsorption. The normal velocity used by the superabsorbing algorithm in Equation (3.23), c, is assumed to correspond to $\varepsilon_{r,eff} = 9.6$ in each case. The single-speed first-order Mur also assumes that $\varepsilon_{r,eff} = 9.6$ to calculate v.

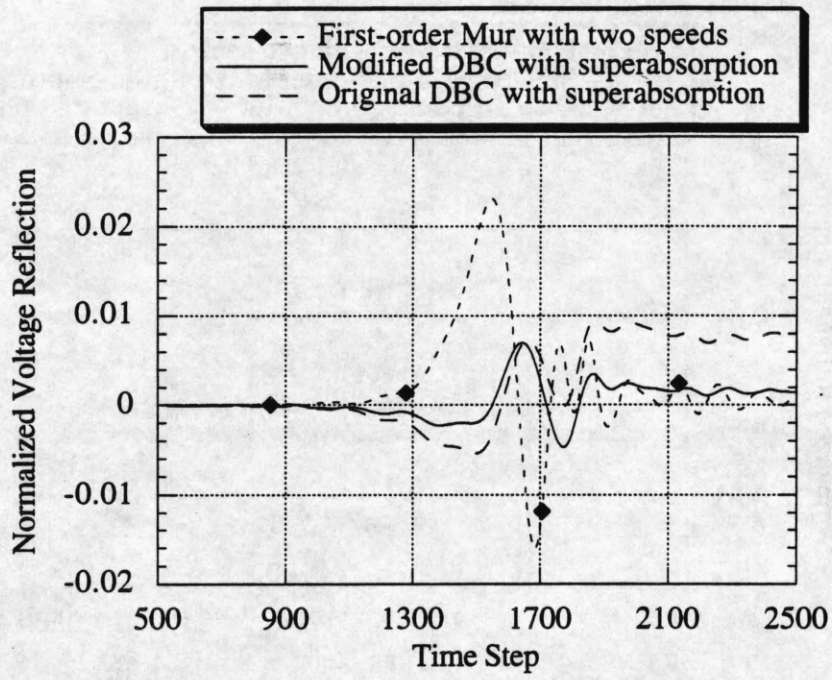

(a)

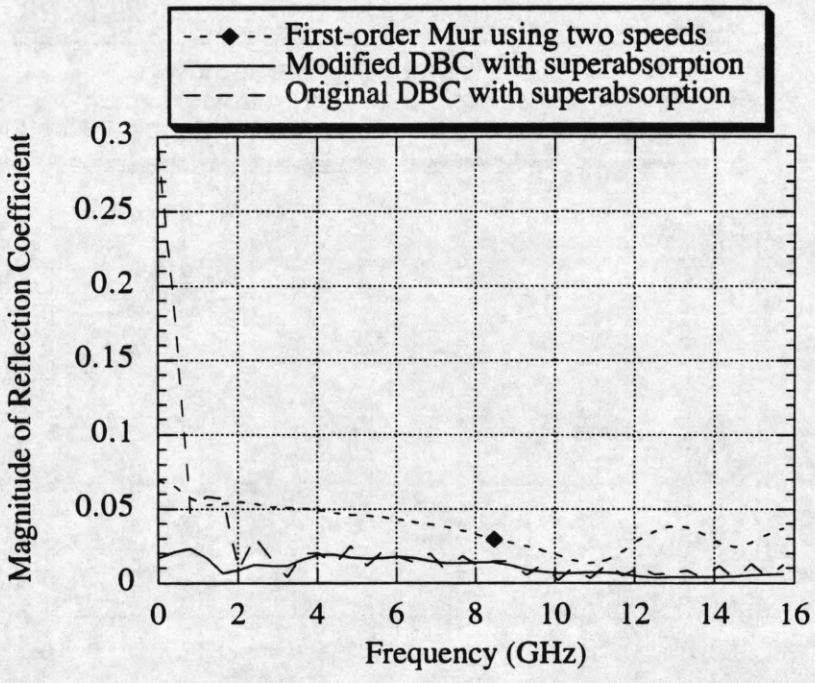

(b)

Figure 3.10 Reflection in the (a) time domain and (b) frequency domain from the original and modified DBCs when superabsorption is applied. In both cases, c for the superabsorption algorithm is chosen by assuming $\varepsilon_{r,eff} = 8.0$, and both DBCs use $\varepsilon_{r,eff1} = 7.12$ and $\varepsilon_{r,eff2} = 8.50$. The modified DBC uses $\alpha_1 = 0.1/\Delta z$ and the reflection from a first-order Mur ABC is shown for comparison.

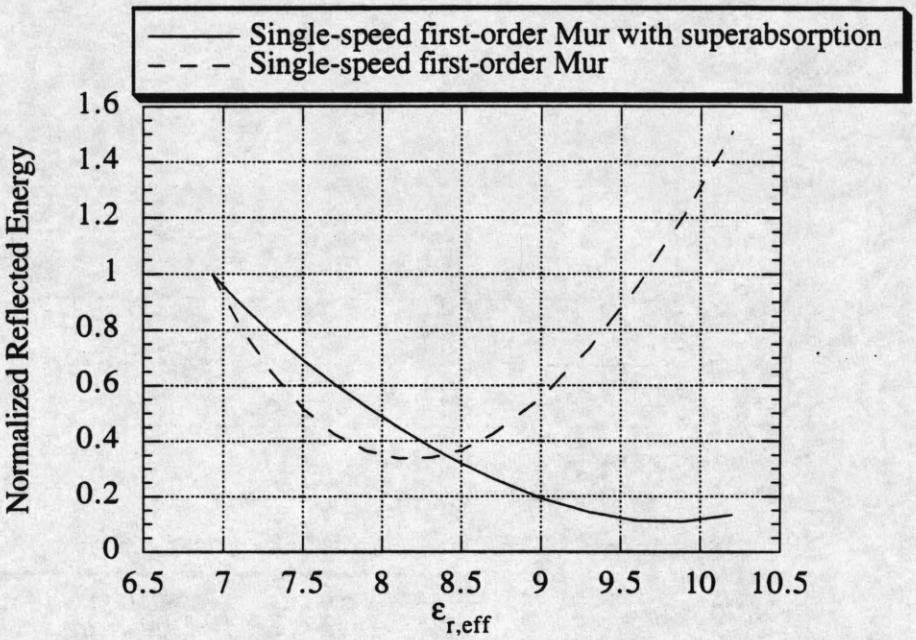

Figure 3.11 Variation of reflected energy of a single-speed first-order Mur with and without superabsorption as the assumed speed of the incident wave changes. The curves are normalized to different values so that sensitivity comparisons may be made; when denormalized, the curve with superabsorption is 29.9 times lower than the curve without superabsorption.

Table 3.1 Comparison of three norms of the reflection caused by various absorbing boundary conditions. The L_1 and L_2 entries for the original DBC are marked with an asterisk because the values given here are those obtained from a reflection signal that ended at $t = 2500\Delta t$. Since the reflection for these signals did not go to zero at large times, these two norms would be infinite if the simulation could be extended indefinitely.

Boundary Condition	**L_2 Norm**	**L_∞ Norm**	**L_1 Norm**
Single-speed first-order Mur with superabsorption applied	0.0574	0.00334	1.68
Dual-speed first-order Mur with superabsorption applied	0.0909	0.00781	2.13
Modified DBC with superabsorption applied	0.0915	0.00702	2.88
Modified DBC	0.223	0.0145	6.51
Dual-speed first-order Mur	0.285	0.0230	6.43
Single-speed first-order Mur	0.341	0.0232	9.34
Original DBC with superabsorption applied	0.233*	0.00946	7.80*
Original DBC	0.313*	0.0169	10.6*
Second-order Mur	7.96	0.605	172.5

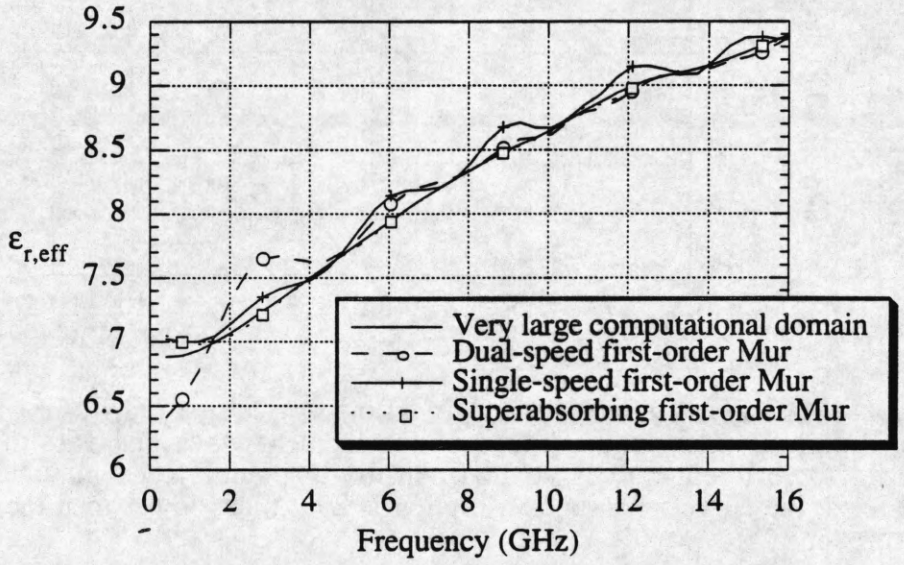

Figure 3.12 Effect of absorbing boundary conditions on computed $\varepsilon_{r,eff}$ curves. The single-speed first-order Mur chooses v by assuming that $\varepsilon_{r,eff} = 7.0$. The single-speed first-order Mur with superabsorption chooses v and c by assuming that $\varepsilon_{r,eff} = 9.6$.

CHAPTER 4

BOUNDARY CONDITIONS TO ABSORB BOTH TRAVELING AND EVANESCENT WAVES

The field behavior near the walls terminating an FDTD simulation of microstrip near the side, or transverse, walls is quite different from that on the end walls. Although the fields impinging upon the side walls are primarily evanescent, they have, nonetheless, some contribution from surface waves that propagate outwards. Furthermore, many problems of interest involve some type of discontinuity in the microstrip, and the fields scattered by the discontinuity will, in general, contain radiated waves that propagate toward the side walls. It is essential, therefore, that the boundary condition enforced on the side walls absorb both traveling and evanescent waves.

Typically the characterization of microstrip via the FDTD method is carried out by terminating the side walls with ABCs which absorb only traveling waves. Such simulations can produce acceptable results only if the side walls are sufficiently far away from the microstrip conductor that evanescent modes are negligible near them. To meet this requirement it is often necessary to use a large computational domain, which greatly increases both computer storage and run-time requirements.

This chapter begins by considering the one-way wave equation of Chapter 2, and shows how the standard approximations used to generate traveling-wave ABCs will not absorb evanescent waves. Two boundary conditions capable of absorbing evanescent waves are proposed and tested. One of these boundary conditions absorbs only evanescent waves, and is shown to be poorly suited to the modeling of microstrip structures, while the other can absorb both evanescent and traveling waves and performs well in microstrip simulations. A recent paper by Betz and Mittra [19] provides a condensed version of much of this chapter.

4.1 The Performance of Traveling Wave ABCs Applied to Evanescent Waves

Consider a boundary on the $x = x_{max}$ plane. The outgoing one-way wave equation, written in the Fourier domain, is

$$\left(jk_x + \sqrt{\frac{-\omega^2}{c^2} + k_y^2 + k_z^2} \right) E = 0 \tag{4.1}$$

which is more conveniently rewritten as

$$\left(jk_x + \frac{j\omega}{c} \sqrt{1 - \frac{c^2 k_y^2}{\omega^2} - \frac{c^2 k_z^2}{\omega^2}} \right) E = 0. \tag{4.2}$$

Now the form of the dominant fields propagating along a z-directed microstrip is

$$E(x, y, z, t) = e^{(j\omega t + jk_z z - \alpha_x x - \alpha_y y)}. \tag{4.3}$$

Comparison with the plane-wave form given by (2.2) shows that $k_x = j\alpha_x$ and $k_y = j\alpha_y$, where α_x and α_y are positive real numbers. From the dispersion relation, (2.3), and the relations between the transverse wavenumbers and attenuation factors, one finds that

$$\frac{\omega^2}{c^2} - k_z^2 = -\alpha_x^2 - \alpha_y^2. \tag{4.4}$$

Since all the variables in (4.4) are real, it is apparent that

$$\frac{k_z^2 c^2}{\omega^2} > 1. \tag{4.5}$$

Now in order to derive the Mur ABCs, we approximated the square root in (4.2) by the first one or two terms of its Taylor series. However, the Taylor series for $\sqrt{1-x}$ converges only if $|x| < 1$, so from (4.5) we see that a Taylor series approximation of (4.2) cannot converge to the correct answer. Consequently, we do not expect any of the boundary conditions of Chapter 3 to absorb evanescent waves well.

Since the second-order Mur ABC can be written as a dispersive boundary condition, and the first-order Mur is a degenerate case of the DBC, let us find the reflection coefficient of an evanescent wave incident on a DBC. By substituting field behavior of the form

$$E(x,t) = e^{(j\omega t - \alpha_x x)} + Re^{(j\omega t + \alpha_x x)} \tag{4.6}$$

into the analog of (3.10) for the $x = x_{max}$ wall, one finds that

$$\left(-\alpha_x + \frac{j\omega}{v_1}\right)\left(-\alpha_x + \frac{j\omega}{v_2}\right)e^{(j\omega t - \alpha_x x)} + R\left(\alpha_x + \frac{j\omega}{v_1}\right)\left(\alpha_x + \frac{j\omega}{v_2}\right)e^{(j\omega t + \alpha_x x)} = 0. \tag{4.7}$$

Solving for R and neglecting the relative phase term yield

$$R = -\frac{(-\alpha_x v_1 + j\omega)(-\alpha_x v_2 + j\omega)}{(\alpha_x v_1 + j\omega)(\alpha_x v_2 + j\omega)}. \tag{4.8}$$

Since the magnitude of each factor in (4.8) is 1, the DBC completely reflects evanescent waves. Since a second-order Mur ABC can be expressed as a DBC with $v_1 = v_2 = c$, and a first-order Mur is just a single-factor DBC, these two ABCs will also completely reflect evanescent waves.

4.2 Boundary Conditions to Model Evanescent Waves

Since it is the lack of convergence of the Taylor series of the square root term in (4.2) which appears to lead to the inability of the traveling-wave ABCs to model evanescent waves, the reader may ask why one does not factor out the k_z term in (4.1) instead of the ω/c term. This manipulation would yield

$$\left(jk_x + k_z\sqrt{1 - \frac{\omega^2}{c^2 k_z^2} + \frac{k_y^2}{k_z^2}}\right)E = 0. \tag{4.9}$$

The square root term can now be easily expanded in a convergent series, but the facts that k_z no longer has a j in front of it and that multiplication by j would remove the j in front of k_x make it impossible to map the resulting equations back to differential operators in the spatial domain. Clearly a different approach is required.

The attenuation in the transverse direction in a microstrip simulation is not a strong function of frequency; it does not change radically from mode to mode. This suggests that we should approximate the square root term in (4.1) by a constant, yielding

$$(jk_x + \alpha)E = 0, \tag{4.10}$$

which in the spatial domain is

$$\left(\frac{\partial}{\partial x} + \alpha\right)E = 0. \tag{4.11}$$

The reflection coefficient of this ABC is

$$R = -\frac{jk_x + \alpha}{-jk_x + \alpha}. \tag{4.12}$$

Clearly this ABC will absorb evanescent waves, for which $jk_x = -\alpha$, but it completely reflects traveling waves, for which k_x is real. By discretizing (4.11) on the $x = M\Delta x$ boundary one obtains the update equation

$$E_M^n = \frac{(1 - \alpha\Delta x/2)}{(1 + \alpha\Delta x/2)} E_{M-1}^n. \tag{4.13}$$

As mentioned at the start of this chapter, even uniform microstrip simulations contain some surface waves which propagate outwards, and many problems of interest involve discontinuities which will scatter traveling waves. Consequently, boundary condition (4.11) is not very useful.

In order to improve upon boundary condition (4.11), let us add a factor which will absorb traveling waves:

$$\left(\frac{\partial}{\partial x} + \frac{1}{v}\frac{\partial}{\partial t}\right)\left(\frac{\partial}{\partial x} + \alpha\right)E = 0. \tag{4.14}$$

Discretizing this ABC on the $x = M\Delta x$ boundary via central differences yields

$$\begin{aligned} E_M^n = &\left(\frac{1}{2v\Delta t + 2\Delta x + \alpha v\Delta t\Delta x}\right)\cdot\left[(-2v\Delta t + 2\Delta x - \alpha v\Delta t\Delta x)E_M^{n-1}\right. \\ &+ \left(4v\Delta t - 4\alpha\Delta x^2\right)E_{M-1}^n + \left(4v\Delta t + 4\alpha\Delta x^2\right)E_{M-1}^{n-1} \\ &\left. + (-2v\Delta t + 2\Delta x + \alpha v\Delta t\Delta x)E_{M-2}^n + (-2v\Delta t - 2\Delta x + \alpha v\Delta t\Delta x)E_{M-2}^{n-1}\right], \end{aligned} \tag{4.15}$$

where subscripts and superscripts denote the x index and time step, respectively. The reflection coefficient of the continuous boundary condition, (4.14), is

$$R = -\frac{(jk_x + \alpha)(jk_x + j\omega/v)}{(-jk_x + \alpha)(-jk_x + j\omega/v)}. \tag{4.16}$$

Clearly for either evanescent waves, for which $jk_X = -\alpha$, or for outgoing traveling waves, for which k_X is real and negative, the reflection coefficient of this ABC is less than 1.

4.3 Choice of Boundary Condition Parameters

Both the evanescent ABC, (4.11), and the evanescent-traveling ABC, (4.14), require that an attenuation parameter, α, be chosen. In addition, the evanescent-traveling ABC requires a choice of v, the assumed normal velocity of waves incident on the boundary. In this research it was found that ABC (4.14) was not very sensitive to v and that it could be set equal to the speed of light in whatever medium lies next to the boundary. At the boundaries intersected by the microstrip dielectric-air interface, v is set equal to c_o and $c_{dielectric}$ on the portions of the boundaries adjacent to air and dielectric, respectively.

The determination of α is more complex. We use a finite-difference approximation to the Laplace equation to find the static field distribution of the microstrip. The computational domain is made somewhat larger than the corresponding cross-section used in the subsequent FDTD simulation so that we can obtain accurate data at the points where the ABCs will lie in the FDTD simulation. If one assumes the fields behave as $\exp(-\alpha x)$ in the region of $x = M\Delta x$, α is given by

$$\alpha_{x=M\Delta x} = \frac{-1}{E}\frac{\partial E}{\partial x}\bigg|_{x=M\Delta x}. \tag{4.17}$$

It was found in this research that α should be set to one value along each wall; changing the value of α from node to node tends to degrade the ABC's performance. Consequently, we must find some average value of α on each boundary at which we desire to implement an evanescent ABC. Four different averaging schemes were tested in this research: arithmetic and weighted averages of the values of α found by applying (4.17) to either the tangential field or the magnitude of the field over the boundary. The field magnitude in a Laplacian

problem is $\sqrt{E_x^2 + E_y^2}$ and the weighted averages mentioned above are defined by weighting the α value found at each node by the corresponding field strength. Figure 4.1 shows the sensitivity of ABC (4.14) to the value of α in a uniform microstrip simulation; the choices of α recommended by the four averages mentioned above are marked for comparison. The microstrip simulated to generate Figure 4.1 had H = 0.1 mm, W = 0.75 mm, ε_r = 13, a step size of 6.25 μm in each direction, and 24 and 14 cells from the nearest edge of the conductor to the ABCs in the x- and y-directions, respectively.

While each of these four methods provided reasonable values of α, tests of several different microstrips showed that the weighted average of the electric field magnitude method generally gave the best value; the values of α for the simulations discussed in the remainder of this chapter were chosen in this manner. The exact formula used to find α on, for example, the $x = M\Delta x$ boundary is

$$\frac{\frac{1}{2N\Delta x}\sum_{j=1}^{N}|E|(M-1,j)-|E|(M+1,j)}{\sum_{j=1}^{N}|E|(M,j)} \tag{4.18}$$

where |E| is the magnitude of the electric field; the numbers in brackets indicate the x and y indices of the Laplace field nodes, which are assumed to coincide with those of the FDTD simulation; and the side boundaries of the FDTD simulation are at $x = M\Delta x$ and $y = N\Delta y$.

Since the finite-difference solution of the two-dimensional Laplace equation takes a negligible amount of time compared to the time required for the solution of the three-dimensional FDTD problem, the determination of α involves little computational overhead. Although the value of α thus determined is really the quasi-static approximation to a frequency-dependent parameter, an ABC using this α provides good performance through the frequency range that is typically of interest.

4.4 Application of Evanescent ABCs to a Uniform Microstrip Problem

In this section, we test the two ABCs introduced in Section 4.2 by applying them to the side walls of an FDTD simulation of the uniform microstrip described in Section 3.1. Figure 4.2 shows the cross-section of the problem and indicates where the boundary conditions under test are applied.

The error introduced by the side-wall ABCs is determined by comparing the results found with a small computational-domain cross-section of $24\Delta x$ by $24\Delta y$ with that obtained when the computational-domain cross-section is very large, in this case $110\Delta x$ by $70\Delta y$. The larger problem uses second-order Mur ABCs on the side walls, since evanescent waves will be negligible at this distance from the microstrip conductor.

Figure 4.3 compares the performance of the evanescent ABC of Equation (4.11), the combined evanescent-traveling wave ABC of Equation (4.14), and the second-order Mur ABC. Note that in the lower frequency region from 0 to 10 GHz, which is typically of most interest to circuit designers, both evanescent ABCs outperform the second-order Mur condition by a significant margin. Near 12 GHz, however, the second-order Mur ABC introduces less error than either of the other two ABCs. The reason for this is presumably that the source has excited a significant amount of outward propagating surface waves near 12 GHz. The second-order Mur ABC absorbs these waves best, since it contains two terms designed to absorb traveling waves, while the combined evanescent-traveling wave ABC contains only one, and the purely evanescent ABC completely reflects traveling waves. Since we chose α to be the quasi-static value, one would expect the evanescent ABCs to perform best at lower frequencies, which is indeed the case. Furthermore, as the frequency rises guided-wave modes are more highly localized about the microstrip conductor, so evanescent fields are less significant near the absorbing boundary conditions, while surface waves become more significant. Consequently, the fact that the second-order Mur performs about as well as the combined evanescent-traveling wave ABC at high frequencies is understandable. The high frequency performance of the combined evanescent-traveling

wave ABC could be improved by adding more factors to (4.14) to create higher-order boundary conditions. In practice, however, circuit designers are often interested only in the lower-frequency behavior of microstrip structures, so the boundary condition of (4.14) will usually be adequate. The complete inability of the evanescent boundary to absorb traveling waves makes the use of this ABC undesirable; one should always use the ABC of (4.14) instead of (4.11).

4.5 Application to a Gap in Microstrip Line Problem

The second numerical example involves the calculation of the scattering parameters of a microstrip gap from FDTD data [20, 21]. The only two independent scattering parameters for a symmetric two-port problem such as this are S_{11} and S_{21} which are defined by

$$S_{11} = \frac{V_{1,ref}(f)}{V_{1,inc}(f)} \qquad S_{21} = \frac{V_{2,trans}(f)}{V_{1,inc}(f)}. \tag{4.19}$$

In order to find the incident voltage waveform, a uniform microstrip is simulated. By subtracting this waveform from the voltage monitored at port 1 of the simulation of the microstrip with gap geometry one obtains $V_{1,ref}$. $V_{1,trans}$ can be directly monitored at port 2 of the microstrip with gap simulation.

The geometry of the microstrip gap simulation is shown in Figure 4.4. The microstrip conductor width is 0.6 mm, the dielectric thickness is 0.6 mm, and the relative permittivity of the substrate is 9.6. The step size in all directions is 0.06 mm; there is a 0.3 mm gap in the microstrip conductor halfway down the line; and the computational domain cross-section is 24 x 24 cells. Figure 4.5 compares the errors in the magnitudes of S_{11} and S_{21} introduced by the combined evanescent-traveling wave ABC and the second-order Mur boundary condition. These errors are computed via comparison with a simulation run with a computational domain cross-section of 110 x 60 cells. Since evanescent fields are negligible near the side walls in the larger simulation, accurate results can be obtained even if second-

order Mur ABCs are used to terminate the computational domain in the transverse direction, and the results with the larger computational domain are taken as a reference. As in the uniform microstrip example, the combined evanescent-traveling wave ABC provides better results than the second-order Mur ABC. Since radiated fields are significant for discontinuity problems of this type, it should be possible to obtain further improvements in accuracy by adding additional traveling wave factors to (4.14) to create higher-order boundary conditions.

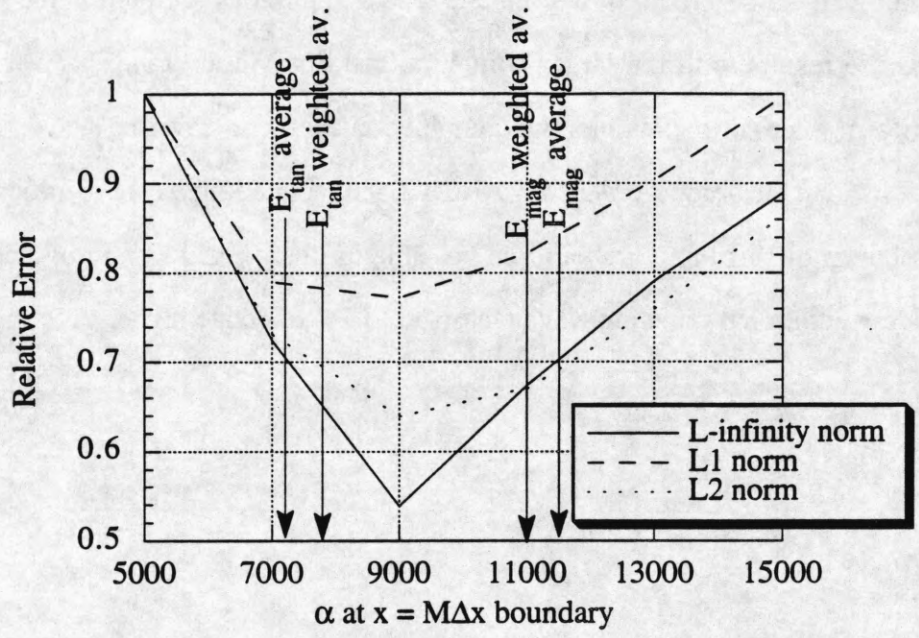

(a)

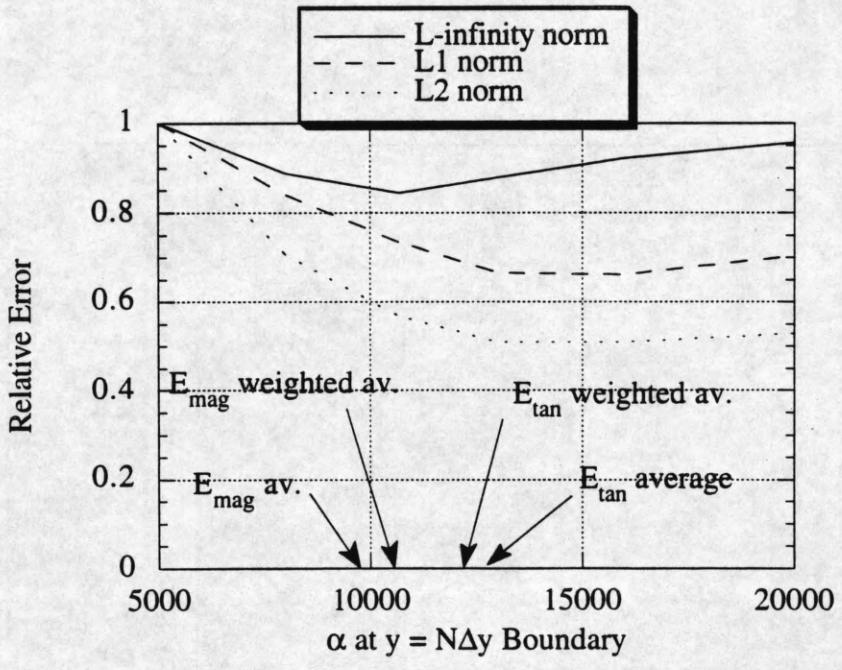

(b)

Figure 4.1 Dependence of error in a uniform microstrip simulation caused by evanescent ABCs on (a) the x = MΔx boundary and (b) the y = NΔy boundary on α. The α values obtained by various averages of the fields found from a Laplace solver are marked for comparison.

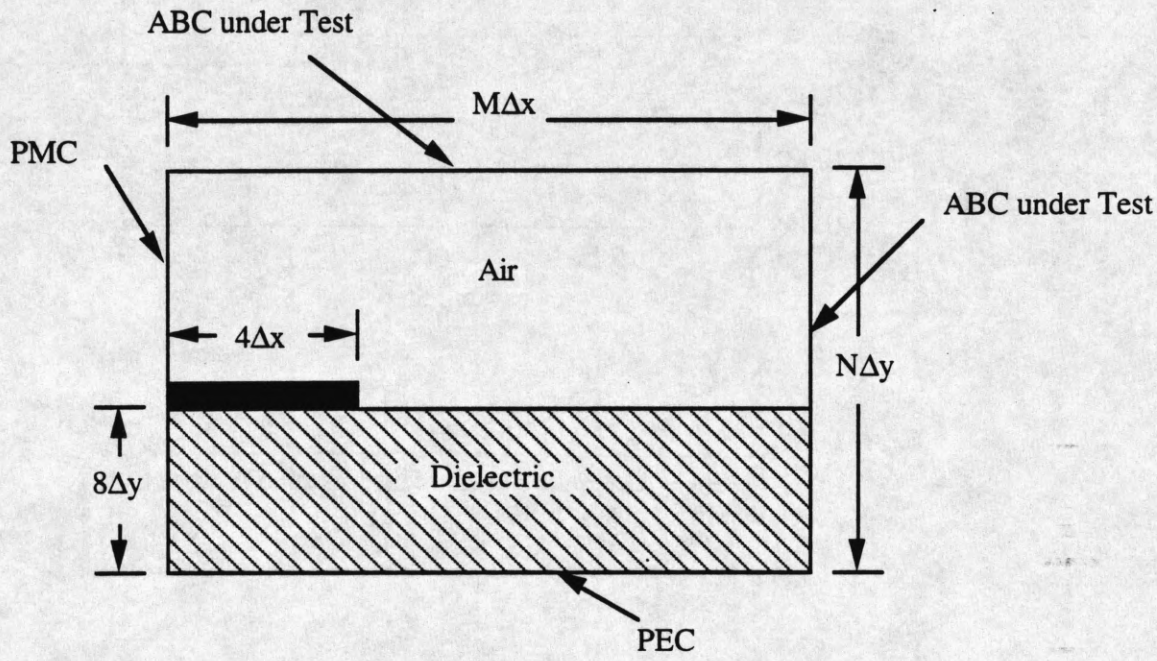

Figure 4.2 Cross-section of the uniform microstrip geometry simulated to test the performance of the evanescent ABCs.

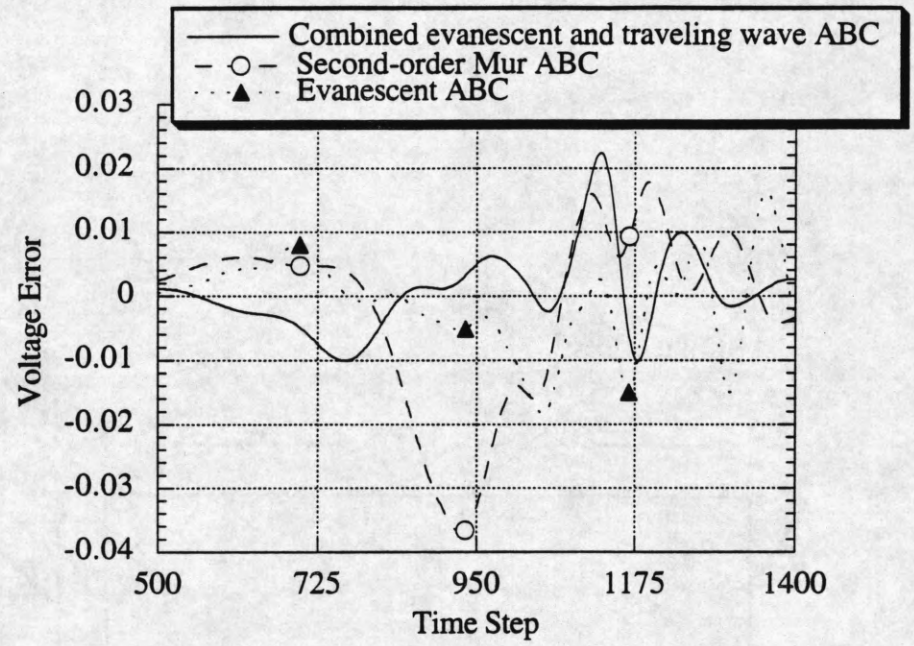

(a)

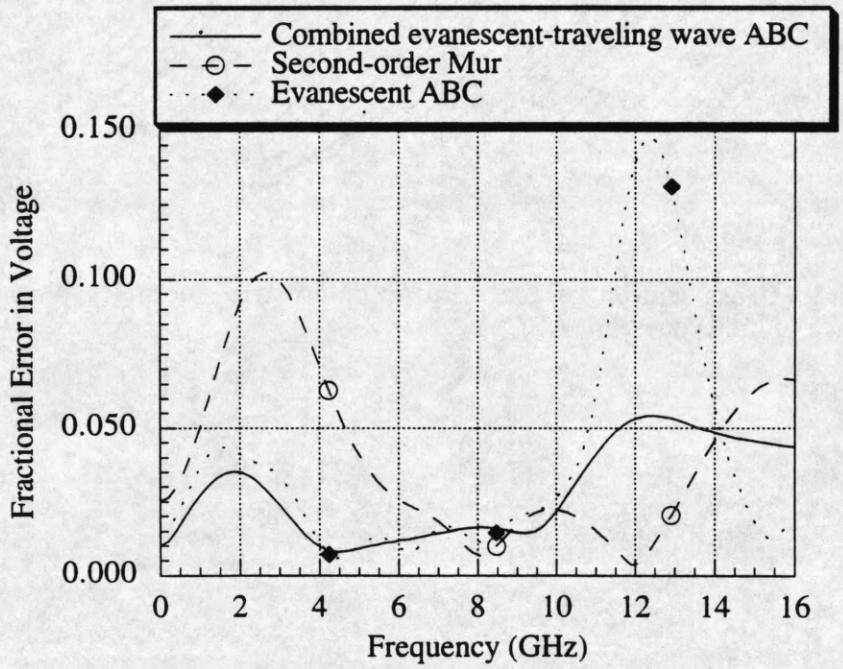

(b)

Figure 4.3 Error introduced by side ABCs into a uniform microstrip simulation in (a) the time-domain, and (b) the frequency-domain. The evanescent-traveling wave and the evanescent ABC use α at $M\Delta x = 281$ and α at $N\Delta y = 237$.

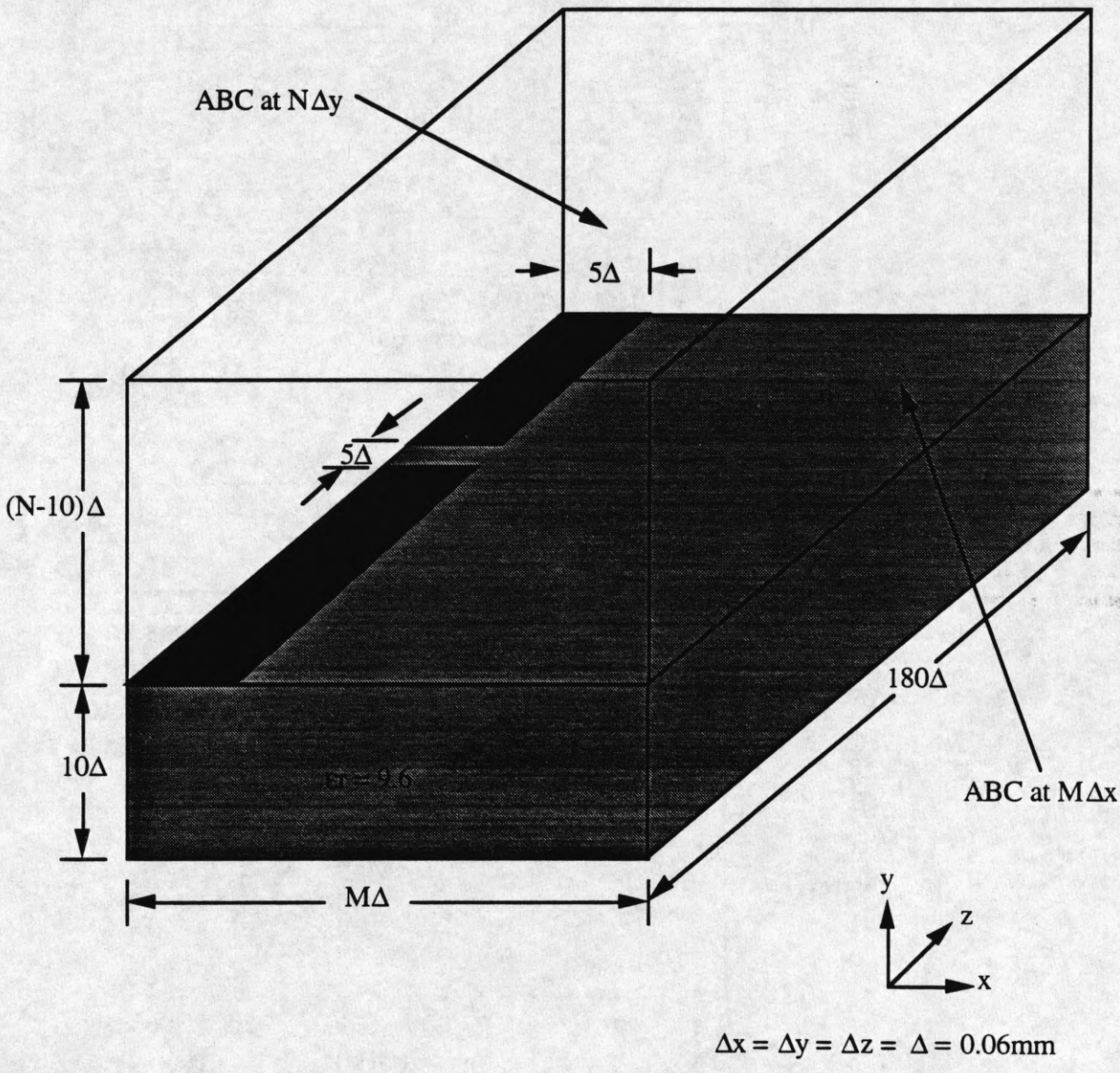

Figure 4.4 Microstrip gap geometry simulated for the scattering parameter example.

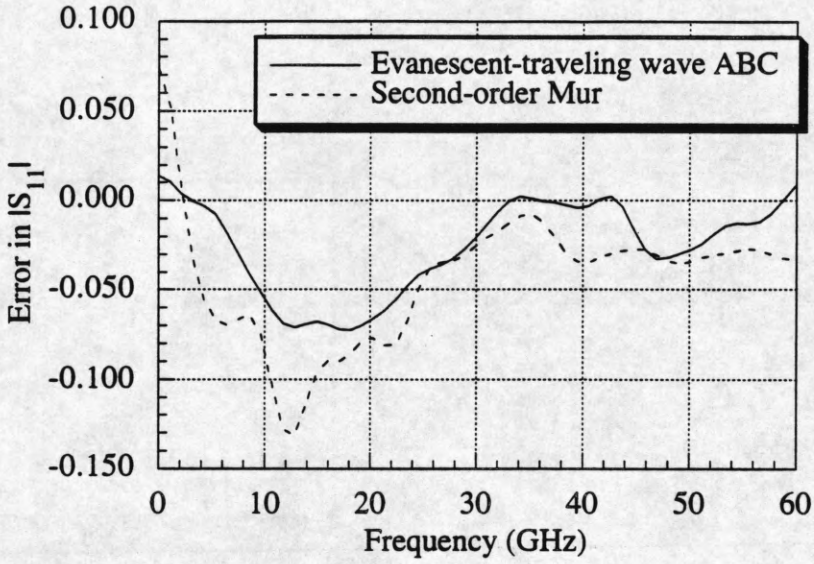

(a)

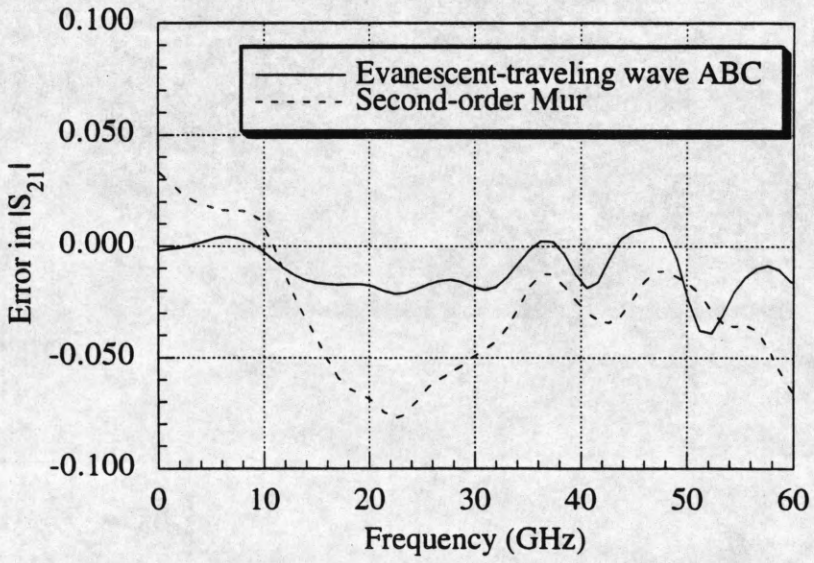

(b)

Figure 4.5 Error in the magnitude of (a) S_{11} and (b) S_{21} of a microstrip gap introduced by different ABCs. The evanescent-traveling wave boundary uses α at $M\Delta x = 1524$ and α at $N\Delta y = 1257$.

CHAPTER 5
CONCLUSIONS

This thesis has described absorbing boundary conditions suitable for truncating an FDTD simulation of microstrip line in both the longitudinal, or guiding, and the transverse, or attenuating, directions. Consider first the ABCs tested on the longitudinal walls of the microstrip; these ABCs must absorb normally incident waves traveling at a fairly wide range of velocities. It was found that the second-order Mur ABC is not suitable for the termination of the guiding ends of a microstrip, as the tangential derivatives inherent in this ABC become undefined as one crosses the conductor boundaries and the dielectric-air interface which make up the microstrip. Litva's dispersive boundary condition was also a disappointment -- this ABC has difficulty absorbing low-frequency signal components. However, a modified DBC obtained by adding an attenuation factor to Litva's DBC did not have these problems near dc, and is more absorbing than the first-order Mur ABC generally used by the EM community today. The superabsorbing boundary algorithm was applied to each of the boundary conditions mentioned above and improved the performance of all of them. The most effective absorbing boundary condition tested was the single-speed first-order Mur ABC with superabsorption applied. For optimal performance, the wave speed assumed by the first-order Mur ABC should be the same as that assumed by the super-absorbing algorithm, and should be based on an estimate of $\varepsilon_{r,eff}$ that is only slightly below the substrate dielectric constant. Heuristic guidelines for choosing the adjustable parameters contained in the first-order Mur and dispersive ABCs were also presented, and the sensitivity of each ABC to its input parameters was investigated. Finally, a numerical example showed the considerable effect that even slight reflections from the end walls can have on the accuracy of $\varepsilon_{r,eff}$ values computed from time-domain data.

The absorbing boundary conditions enforced on the transverse walls should be able to absorb both evanescent and traveling waves, as both can be significant on these planes.

Reflection coefficients derived from the continuous description of ABCs showed that the traveling-wave ABCs currently used by the EM community on the transverse walls completely reflect evanescent waves. Therefore, two new absorbing boundary conditions were proposed: one which absorbs only evanescent waves and one which absorbs both traveling and evanescent waves. In a test of a uniform microstrip, the combined evanescent-traveling wave ABC outperformed the evanescent only ABC, so this is the boundary condition best-suited to the modeling of microstrip components. In FDTD simulations of both a uniform microstrip and a microstrip gap discontinuity, this combined evanescent-traveling wave ABC provided more accurate results than did the second-order Mur ABC, which is the boundary condition most commonly used on the transverse walls of microstrip simulations by the EM community. The wave speed assumed by this evanescent-traveling wave ABC can be set to the speed of light in the material adjacent to the boundary, and the attenuation constant can be determined from the quasi-static field distribution of a microstrip found by a finite-difference Laplace solver. This boundary condition is not overly sensitive to its input parameters, and should therefore be quite robust.

Use of the more advanced absorbing boundary conditions described above will allow FDTD simulations to produce more accurate results on smaller computational domains, resulting in large savings in computer memory and time and allowing larger problems to be simulated. Reduced reflections from the boundary conditions will make frequency-domain parameters computed from FDTD data more accurate and more smoothly varying, since Fourier transforming the time-domain data tends to magnify errors.

Several promising avenues for fruitful research remain, however. As mentioned in Chapter 2, Liao's boundary condition is an excellent absorber of traveling waves, and since it uses only normal derivatives, it may be well-suited to use on the guiding ends of microstrip if its stability problems can be overcome. The modified dispersive boundary condition of Chapter 3 performed very well, and this boundary condition can be easily extended to higher orders by adding more factors to Equation (3.15). If one ensures that enough factors contain

attenuation terms, α_i, the dc behavior of these high-order DBCs should remain stable, and the higher the order of the DBC, the better its performance at other frequencies should be. Similarly, the combined evanescent-traveling wave ABC could be extended to higher orders by adding more factors to Equation (4.14), some to absorb traveling and some to absorb evanescent waves.

REFERENCES

[1] K. S. Yee, "Numerical solution of initial boundary value problems involving Maxwell's equations in isotropic media," *IEEE Trans. Antennas Propagat.*, vol. AP-14, pp. 302-307, May 1966.

[2] B. Engquist and A. Majda, "Absorbing boundary conditions for the numerical simulation of waves," *Math. Comp.*, vol. 31, pp. 629 - 651, July 1977.

[3] L. N. Trefethen and L. Halpern, "Well-posedness of one-way wave equations and absorbing boundary conditions," *Math. Comp.*, vol. 47, pp. 421-435, October 1986.

[4] G. Mur, "Absorbing boundary conditions for the finite-difference approximation of the time-domain electromagnetic-field equations," *IEEE Trans. Electromagn. Compat.*, vol. EMC-23, pp. 377-382, Nov. 1981.

[5] E. L. Lindman, "Free-space boundary conditions for the time dependent wave equation," *J. Comp. Phys.*, vol. 18, pp. 66-78, May 1975.

[6] W. C. Chew, *Waves and Fields in Inhomogeneous Media.* New York: Van Nostrand Reinhold, 1990, pp. 246-256.

[7] Z. P. Liao, H. L. Wong, B. P. Yang, and Y. F. Yuan, " A transmitting boundary for transient wave analyses," *Scientia Sinica (Series A)*, vol. 27, pp. 1063-1076, October 1984.

[8] M. Moghaddan and W. C. Chew, "Stabilizing Liao's absorbing boundary conditions using single-precision arithmetic," *IEEE AP-S Int. Symp.*, London, ON, Canada, June 24-28, 1991, pp. 430-433.

[9] V. Betz and R. Mittra, "Comparison and evaluation of boundary conditions for the absorption of guided waves in an FDTD simulation," *IEEE Trans. Microwave Guided Wave Lett.*, vol. 2, pp. 499-501, Dec. 1992.

[10] R. L. Higdon, "Numerical absorbing boundary conditions for the wave equation," *Math Comp.*, vol. 49, pp. 65-90, July 1987.

[11] J. Fang, "Investigation on the stability of absorbing boundary conditions for the time-domain finite-difference method," *IEEE AP-S Int. Symp.*, Chicago, IL, July 18-25, 1992, pp. 548-551.

[12] K. C. Gupta, R. Garg, and R. Chadha, *Computer-Aided Design of Microwave Circuits.* Norwood, MA: Artech House, 1981, pp. 60-64.

[13] R. L. Higdon, "Absorbing boundary conditions for difference approximations to the multi-dimensional wave equation," *Math Comp.*, vol. 47, pp. 437-459, Oct. 1986.

[14] Z. Bi, K. Wu, C. Wu, and J. Litva, "A dispersive boundary condition for microstrip component analysis using the FDTD method," *IEEE Trans. Microwave Theory Tech.*, vol. 40, pp. 774-777, Apr. 1992.

[15] J. Fang and K. K. Mei, "A super-absorbing boundary algorithm for solving electromagnetic problems by time-domain finite-difference method," *IEEE AP-S Int. Symp.*, Syracuse, NY, June 6-10, 1988, pp. 472-475.

[16] K. K. Mei and J. Fang, "Superabsorption -- a method to improve absorbing boundary conditions," *IEEE Trans. Antennas Propagat.*, vol. AP-40, pp. 1001-1010, Sept. 1992.

[17] C. T. Chen, *Linear System Theory and Design*. New York: Holt, Rinehart and Winston, 1984, p. 57.

[18] X. Zhang, J. Fang, K. K. Mei, and Y. Liu, "Calculations of the dispersive characteristics of microstrips by the time-domain finite difference method," *IEEE Trans. Microwave Theory Tech.*, vol MTT-36, pp. 263-267, Feb. 1988.

[19] V. Betz and R. Mittra, "A boundary condition to absorb both propagating and evanescent waves in a finite-difference time-domain simulation," *IEEE Trans. Microwave Guided Wave Lett.*, vol. 3, pp. 182-184, June 1993.

[20] X. Zhang and K. K. Mei, "Time-domain finite difference approach to the calculation of the frequency-dependent characteristics of microstrip discontinuities," *IEEE Trans. Microwave Theory Tech.*, vol. 36, pp. 1775-1787, Dec. 1988.

[21] D. M. Sheen, S. M. Ali, M. D. Abouzahra, and J. A. Kong, "Application of the three-dimensional finite-difference time-domain method to the analysis of planar microstrip circuits," *IEEE Trans. Microwave Theory Tech.*, vol. 38, pp. 849-857, July 1990.